

Southern GEMS groups II: HI distribution, mass functions and HI deficient galaxies^{*}

Virginia A. Kilborn^{1,2†}, Duncan A. Forbes¹, David G. Barnes^{1,3}, Bärbel S. Koribalski², Sarah Brough¹, and Katie Kern^{1,2}

¹Centre for Astrophysics & Supercomputing, Swinburne University of Technology, Mail H39, PO Box 218, Hawthorn, VIC 3122, Australia

²Australia Telescope National Facility, CSIRO, P.O. Box 76, Epping, NSW 1710, Australia

³School of Physics, University of Melbourne, Parkville, VIC 3010, Australia

ABSTRACT

We investigate the neutral hydrogen (HI) content of sixteen groups for which we have multi-wavelength data including X-ray observations. Wide-field imaging of the groups was obtained with the 20-cm multibeam system on the 64-m Parkes telescope. We have detected ten previously uncatalogued HI sources, one of which has no visible optical counterpart. We examine the HI properties of the groups, compared to their X-ray characteristics, finding that those groups with a higher X-ray temperature and luminosity contain less HI per galaxy. The HI content of a group depends on its morphological make-up, with those groups dominated by early-type galaxies containing the least total HI. We determined the expected HI for the spiral galaxies in the groups, and found that a number of the galaxies were HI deficient. The HI deficient spirals were found both in groups with and without a hot intra-group medium. The HI deficient galaxies were not necessarily found at the centre of the groups, however, we did find that two thirds of HI deficient galaxies were found within about 1 Mpc from the group centre, indicating that the group environment is affecting the gas-loss from these galaxies. We determined the HI mass function for a composite sample of 15 groups, and found that it is significantly flatter than the field HI mass function. We also find a lack of high HI-mass galaxies in groups. One possible cause of this effect is the tidal stripping of HI gas from spiral galaxies as they are pre-processed in groups.

Key words: Galaxies: evolution, interactions, mass function, clusters:general, X-rays: galaxies

1 INTRODUCTION

Environment has an important effect on the evolution of galaxies. The observation of Butcher & Oemler (1978) that high-redshift clusters contain a much higher percentage of blue spiral galaxies than present-day clusters indicates possible evolution and transformation of spirals in the densest regions of the Universe. Further evidence is seen in the star formation rates of galaxies in clusters which are much lower than those galaxies of similar morphology in the field (e.g. Lewis et al. 2002; Gomez et al. 2003). One outstanding question is whether spiral galaxies are somehow transformed

into the present-day lenticular, or S0, galaxies. The mechanism for such a transformation is still not clear: Stripping, interactions, and the cessation of star formation leading to the fading of a spiral disk have all been proposed (Wilman 2009).

It is now accepted that the galaxy group environment plays an important influence on the evolution of galaxies. Star formation is suppressed with respect to the field, in galaxies which lie in densities equivalent to the group environment (Lewis et al. 2002; Gomez et al. 2003), and over half of all galaxies live in the group environment (Eke et al. 2004). Intra-group X-rays are observed in dynamically evolved groups, and these groups also tend to have a central, bright elliptical galaxy and high early-type fraction in the group (e.g. Mulchaey & Zabludoff 1998), similar as is seen in the much denser, and rarer cluster environment.

One of the first signs of a spiral galaxy undergoing a

^{*} The observations were obtained with the Australia Telescope which is funded by the Commonwealth of Australia for operations as a National Facility managed by CSIRO.

[†] E-mail: vkilborn@swin.edu.au

transformation is the cessation of star formation, and the loss of cool gas. The latter is detectable via observations of the neutral hydrogen (HI) in spiral galaxies. It is well-known that spiral galaxies in rich clusters tend to contain less HI than field spirals of similar morphology and size - these galaxies are “HI deficient” (e.g. Magri et al. 1998; Cayatte et al. 1990; Solanes et al. 2001; Gavazzi et al. 2005). There have been several claims of a similar HI deficiency detected in loose groups of galaxies (Sengupta et al. 2007; Sengupta & Balasubramanyam 2006; Kilborn et al. 2005; Omar & Dwarakanath 2005; Chamaraux & Masnou 2004). Galaxy groups are the ideal environment for galaxy-galaxy interactions due to the low relative velocities of the galaxies, and coupled with the observation of HI deficient galaxies in groups where there is no hot intra-group gas, galaxy interactions could be a way of removing HI from spiral galaxies. However, the detection of ram pressure stripping of a galaxy in a loose group (Rasmussen, Ponman & Mulchaey 2006) begs the question of the frequency and significance of this process. Such a question can only be answered by a consistent blind HI survey of loose groups, in combination with multi-wavelength data, including X-ray data.

As the HI distribution of galaxies changes with environment, so does the HI mass distribution (hereafter HI mass function). The HI Parkes All Sky Survey (HIPASS) shows a trend for a steepening low-mass slope in denser environments (Zwaan et al. 2005). Conversely, Springob, Haynes & Giovanelli (2005) find the low-mass slope flattens with denser environment. Both studies have biases however - the HIPASS sample used only HI detected galaxies to measure the density of the environment, and the Springob, Haynes & Giovanelli (2005) study was based on an optically selected sample of galaxies. There have been a limited number of blind HI studies of groups and clusters. Freeland et al. (2009) found an HI mass function with a low-mass slope consistent with being flat in a blind survey of eight groups, and a flat low-mass slope has also been observed in both the Virgo cluster (Davies et al. 2004; Rosenberg & Schneider 2002) and the Canis Venatici region (Kovac, Oosterloo & van der Hulst 2005). Conversely, a steep low-mass slope was found for the Centaurus A group (Banks et al. 1999).

To address some of the issues and inconsistencies detailed above, we are conducting a study on the effect of the group environment on galaxies, the Group Evolution Multi-Wavelength Study (GEMS; Osmond & Ponman 2004; Forbes et al. 2006). In particular, we have conducted a wide-field HI imaging study of sixteen nearby GEMS groups, using the Parkes radiotelescope. Our data gives us optically unbiased HI observations of a $\sim 5.5^\circ \times 5.5^\circ$ region around the groups, and a velocity coverage of $\sim 2000 \text{ km s}^{-1}$. Brough et al. (2006b) studied the dynamics, group membership, and optical properties of the sixteen groups. In this paper we detail the HI properties of the sixteen groups, and we probe the HI mass function in groups and surrounding environment.

All velocities quoted are heliocentric, in the optical convention, and we use $H_0 = 70 \text{ km s}^{-1} \text{ Mpc}^{-1}$.

2 SAMPLE SELECTION AND DATA REDUCTION

The full GEMS sample includes 60 galaxy groups, chosen from ten optical catalogues, the majority with recession velocities between $1000\text{--}3000 \text{ km s}^{-1}$ and with a ROSAT PSPC exposure time of more than 10,000s within $20'$ of the group position. The full selection criteria are given in Osmond & Ponman (2004) and Forbes et al. (2006). We chose 16 groups that were near or South of Declination 0° , for wide-field HI imaging at Parkes. The groups selected for HI observations have a variety of X-ray properties, from just the central galaxy being detected (6 groups), to diffuse group-scale X-ray emission (8 groups), to no X-ray detection at all (2 groups). Properties of the sixteen observed groups are given in Table 1, including the number of members, X-ray and HI parameters, and early-type fraction. Observing parameters for the groups, including central observing position, central observing velocity, and number of galaxies detected in HI are given in Table 2. We also list the distance to each group from Brough et al. (2006b), who find the most accurate distance available to each group either from surface brightness fluctuation measurements, globular cluster luminosity functions, or the corrected mean group velocity.

2.1 Parkes observations and data reduction

Wide-field HI imaging of the sixteen groups was undertaken at the Parkes radio-telescope from 2000-2003. A $5.5^\circ \times 5.5^\circ$ region around each group centre was surveyed, and $\sim 20h$ of data was obtained for each group. A basket-weave observing pattern was used for the observations (e.g. Barnes & de Blok 2001), where scans were made at a rate of one degree per minute, along lines of equatorial latitude and longitude, separated by 4 arcmin. We used 8MHz filters, with 2048 channels, providing unsmoothed spectral resolution of 3.9 kHz, or 0.83 km s^{-1} .

The data were reduced using the AIPS++ packages LIVEDATA and GRIDZILLA. LIVEDATA was used to correct for the bandpass, and a tukey filter was applied to reduce ringing and noise in the data (Barnes et al. 2001). Bandpass correction was applied on a per-beam, per-scan basis, by iteratively clipping the data and fitting a 2nd degree polynomial to the time series of each channel. We masked out data within 20 arcmin of known HI sources in the field (based on a first, quick process and search step), preventing contamination of the calculated bandpass. Each bandpass-corrected spectrum was frame-shifted to the barycenter of the Earth-Sun system, and then baseline corrected by subtracting a source-masked, iterative, clipped 2nd-degree polynomial fit, this time in the spectral domain.

The GRIDZILLA task was used to image the data. We used the WGTMED statistic, which calculates mesh pixel values by taking the weighted median of data within 6 arcmin of the centre of each pixel. The weight values were directly proportional to the canonical, Gaussian observing beam profile which has a FWHM of 14.4 arcmin. The pixel width in the final cubes is 4 arcmin. The final cubes were smoothed to a spectral resolution of 13.2 km s^{-1} for the searching process, and the rms noise level for each cube is given in Table 2. The average rms noise in the cubes is $7.6 \pm 2.9 \text{ mJy beam}^{-1}$ per

Table 1. Details of the sixteen groups

Group	No. of gals	$\log_{10} L_X(R_{500})$ [erg s ⁻¹]	T_X [keV]	HI_{tot} [10 ⁸ M _⊙]	X-ray Emission	Central gal. type	f_{early}
(1)	(2)	(3)	(4)	(5)	(6)	(7)	(8)
NGC 524	16	41.33 ± 0.05	0.65 ± 0.07	1.6 ± 0.5	Galaxy	E	0.56 ± 0.15
NGC 720	6	41.43 ± 0.02	0.52 ± 0.03	...	Group	E	0.67 ± 0.19
NGC 1052	29	40.53 ± 0.15	0.41 ± 0.15	166.5 ± 3.1	Galaxy	E	0.17 ± 0.34
NGC 1332	10	40.93 ± 0.02	0.56 ± 0.03	40.3 ± 1.7	Galaxy	E	0.80 ± 0.09
NGC 1407	24	41.92 ± 0.02	1.02 ± 0.04	5.2 ± 0.7	Group	E	0.91 ± 0.03
NGC 1566	4	40.85 ± 0.05	0.70 ± 0.11	41.8 ± 2.0	Galaxy	E	0.75 ± 0.12
NGC 1808	6	< 40.59	...	132.2 ± 3.1	Undetected	L	0.00 ± 0.71
NGC 3557	14	42.11 ± 0.04	0.24 ± 0.02	117.5 ± 4.6	Group	E	0.60 ± 0.18
NGC 3783	9	40.94 ± 0.11	...	118.5 ± 6.9	Group	L	0.00 ± 0.50
NGC 3923	30	41.07 ± 0.02	0.52 ± 0.03	182.5 ± 4.3	Galaxy	E	0.33 ± 0.27
NGC 4636	17	41.71 ± 0.02	0.84 ± 0.02	12.6 ± 1.0	Group	E	0.42 ± 0.17
NGC 5044	32	43.09 ± 0.01	1.21 ± 0.02	96.1 ± 3.3	Group	E	0.75 ± 0.05
NGC 7144 [†]	40.71 ± 0.13	Galaxy
NGC 7714	4	< 40.48	0.46 ± 0.07	114.7 ± 10.4	Undetected	L	0.00 ± 1.00
HCG 90	38	41.79 ± 0.05	0.39 ± 0.04	112.4 ± 4.7	Group	E	0.36 ± 0.17
IC 1459	10	41.46 ± 0.04	...	221.5 ± 5.5	Group	E	0.29 ± 0.27

[†]Brough et al. (2006b) did not find any members of this group using the friends-of-friends algorithm.

The columns are (1) Group name; (2) Number of group members according to the Brough et al. (2006b) friends-of-friends algorithm; (3) X-ray luminosity within R_{500} from Osmond & Ponman (2004) (erg s⁻¹); (4) X-ray temperature of the group from Osmond & Ponman (2004) (keV); (5) Total HI mass of the group from this work (10⁸ M_⊙); (6) X-ray emission type of the group; (7) Central galaxy type; (8) Early-type fraction of the group (Brough et al. 2006b).

Table 2. Summary of the HI observations and results.

Group	α, δ (J2000) [^h m], [^o ']	v_{sys} [km s ⁻¹]	Dist. [Mpc]	Obs time [h]	rms [mJy beam ⁻¹]	Detectability [mJy beam ⁻¹]	#HI	#New	#New z
(1)	(2)	(3)	(4)	(5)	(6)	(7)	(8)	(9)	(10)
NGC 524	01 24, +09 26	2632	22.3	22	6.6	25	9	0	0
NGC 720	01 52, -13 34	1717	25.7	20	6.9	22	8	1	0
NGC 1052	02 40, -08 08	1438	18.0	28	5.6	18	15	1	0
NGC 1332	03 26, -21 17	1449	20.9	20	7.7	25	16	0	0
NGC 1407	03 40, -18 37	1695	20.9	21	9.1	25	8	0	0
NGC 1566	04 16, -55 35	1246	21	20	7.8	20	13	0	2
NGC 1808	05 08, -37 36	1141	17	24	6.0	18	7	0	0
NGC 3557	11 09, -37 30	2979	42.5	27	6.0	20	13	0	3
NGC 3783	11 37, -37 53	2819	36	13	15.7	28	12	3 [†]	1
NGC 3923	11 50, -28 46	1497	21.3	20	7.0	25	13	1	0
NGC 4636	12 42, +02 41	1696	13.6	31	5.0	15	22	0	0
NGC 5044	13 15, -16 23	2379	29.0	24	6.4	18	23	3	3
NGC 7144	21 53, -48 28	1880	22.8	22	5.7	18	8	0	6
NGC 7714	23 36, +02 05	2908	39	20	14.0	...	7	1	0
HCG 90	22 02, -32 06	2557	36	21	6.9	25	12	0	0
IC 1459	22 57, -36 36	1672	27.2	23	5.8	18	18	0	0
Total							204	10	15

[†]One of these newly detected galaxies was found in follow-up ATCA data, not the original Parkes survey.

The columns are (1) Group name; (2) Central position of the HI cube; (3) Central velocity of the group (km s⁻¹); (4) Distance to the group in Mpc from Brough et al. (2006b); (5) Approximate integration time (hours); (6) rms noise per channel in the final HI cube, smoothed to a velocity resolution of 13.2 km s⁻¹ (mJy beam⁻¹); (7) Detectability of synthetic Gaussian sources as described in the text (mJy beam⁻¹); (8) Number of HI detections; (9) Number of previously uncatalogued (“new”) detections; (10) Number of new redshifts of previously catalogued galaxies.

channel, but two cubes had significantly greater rms noise of $15.7 \text{ mJy beam}^{-1}$ per channel for the NGC 3783 cube (see Kilborn et al. 2006), and $14.0 \text{ mJy beam}^{-1}$ per channel for the NGC 7714 cube, due to solar interference in the data.

2.2 Source finding and completeness

The Parkes H I cubes were searched visually for sources using the KARMA suite of visualisation packages. Each cube was searched three times in R.A.–Dec., R.A.–velocity and Dec.–velocity projections, and two people searched each cube for sources. The number of H I sources detected in each cube is given in Table 2. Sources visible in each projection, and with a peak flux of $\gtrsim 3\sigma$ were catalogued as sources.

To determine the completeness in each cube, we added synthetic sources to each H I cube, and noted the detection rate for different peak flux and velocity widths of the sources. The synthetic sources were Gaussian in profile, and had peak fluxes of 10, 15, 18, 20, 22, 25, 30 mJy. For each peak flux, three synthetic sources were added to the cube, with velocity width of 50, 150 and 300 km s^{-1} . We define the detectability of the cube, as the peak flux at above which all synthetic sources were recovered, regardless of velocity width. Extra synthetic sources were inserted to the NGC 3783 cube, as its rms noise was much higher than the other cubes. In this case, the synthetic sources had the peak flux values of 25, 28, 30, 32 and 35 mJy. We were unable to determine a detectability limit for the NGC 7714 cube. This cube suffers from significant solar interference, and the rms noise varies across the cube. We therefore exclude this cube from the H I mass function calculations. The detectability of each cube is listed in Table 2. In general the detectability is $\sim 3\sigma$ above the noise, but not in every case.

2.3 Parameterisation of the sources, and flux comparison with HICAT

Once the sources were catalogued as above, an interactive fitting program using MIRIAD routines was run to determine the central position, heliocentric velocity, velocity widths (50% and 20%), integrated flux, peak flux density, and rms noise of the spectrum. Firstly MOMENT was used to make a flux integrated H I distribution map of each source, and IMFIT was then invoked to determine the central position and extent of the source by fitting a 2-dimensional Gaussian profile to the H I distribution. This central position was then used in the task MBSPECT to determine all the other parameters for the source. The resolution of the cube for this step was 6.6 km s^{-1} . The flux of the source was calculated using 3 boxes of 3, 5 and 7 pixels in width around the source, to determine if any sources were extended rather than point sources. Those sources with an increase of $> 20\%$ in flux between the fit from 5 and 7 pixels were flagged as extended, and the box width was increased in the fit of these sources until a stable flux was determined for the source. The H I parameters for the sources in each group are listed in Appendix A.

A number of the GEMS sources overlap with the HIPASS catalogue, HICAT (Meyer et al. 2004). We compared all H I parameters for the sources common to the two surveys, and found excellent agreement in systemic velocity,

flux, position and velocity widths. The majority of fluxes agree within $< 30\%$, and those that have a larger error than this can generally be explained by confusion, or poor baselines in the HICAT spectra. We note, that the velocity resolution for fitting the GEMS sources is 6.6 km s^{-1} , compared to 26.4 km s^{-1} for HICAT.

2.4 Optical matching to H I sources and definition of the groups

The 6dFGS 2DR (Jones et al. 2005) and NED databases were used to obtain the previously catalogued optical galaxies, with optical redshifts in a $\sim 5.5^\circ \times 5.5^\circ$ region around each group centre to match the H I detections to optical galaxies. Full details of the optical detections in the groups are given in Brough et al. (2006b). We matched our H I sources to optical galaxies by searching for galaxies nearby in position and velocity. The matched optical counterparts to the H I detections are given in Appendix B. In the case where there were two or more optically catalogued galaxies near the position of the H I detection, and at the same velocity, then all of these are listed. In some cases there were previously catalogued galaxies with no known redshift - we tentatively include these with a redshift in our list, but they need to be confirmed with higher resolution H I observations or optical confirmation of the redshift. Table 2 lists the number of H I detections, new detections, and new redshifts found in each of the cubes.

2.5 ATCA follow-up observations

We obtained high resolution images of a number of new galaxies and confused sources at the Australia Telescope Compact Array between 2003–2006. The results from the follow-up survey are presented in McKay et al. (2004); Kilborn et al. (2005, 2006) and Kern et al. (2008). For this paper, we use the Parkes H I positions and fluxes. Those sources with ATCA follow-up observations are noted in Appendix B.

2.6 Previously uncatalogued galaxies

We detected ten previously uncatalogued galaxies, and their GEMS names and details are listed in Table 3, along with a reference to detailed maps and descriptions where available. We have made high resolution ATCA observations of seven of the new Parkes detections. In addition to these new detections, we also identified a new dwarf galaxy in follow-up ATCA observations of the spiral galaxy ESO 378-G 011 in the NGC 3783 group. This galaxy was named ATCA_1134-37, and the data for this detection is detailed in Kilborn et al. (2006). Figure 1 shows a 10×10 arcminute square region around the position of the Parkes centre for the three previously uncatalogued detections where we do not have ATCA observations. Two out of three of these new detections have a probable optical counterpart visible in the field, whereas there is no obvious optical counterpart in the GEMS_N7714_7 field. Further high resolution H I observations of this object are required to determine its nature.

The average H I mass of these previously uncatalogued galaxies is $\sim 8 \times 10^8 M_\odot$, so they do not contribute a large

Table 3. New galaxies found in the GEMS HI survey. The columns are as follows: (1) Galaxy name; (2) R.A.(J2000), Dec.(J2000); (3) Heliocentric velocity in the optical convention (km s^{-1}); (4) HI mass; (5) Status of ATCA follow-up observations. (6) Reference where the ATCA data are published and discussed in detail. All quantities are measured from the Parkes data, unless otherwise specified.

GEMS name	$\alpha, \delta(\text{J2000})$ [$^{\text{h}} \text{m}^{\text{s}}$], [$^{\circ} \text{ ' } ''$]	V_{sys} [km s^{-1}]	M_{HI} [$10^8 M_{\odot}$]	ATCA status	Reference
(1)	(2)	(3)	(4)	(5)	
GEMS_N720_6	01:48:58,-12:48:19	1770 ± 7	5.8 ± 0.9	N	...
[MMB2004] J0249-0806	02:49:13,-08:07:18	1419 ± 4	5.8 ± 0.5	Y	McKay et al. (2004)
GEMS_N3783_2	11:31:32,-36:18:53	2733 ± 11	5.8 ± 1.7	Y	Kilborn et al. (2006)
GEMS_N3783_8	11:37:54,-37:56:04	2947 ± 6	21.1 ± 2.9	Y	Kilborn et al. (2006)
GEMS_N3923_11	11:50:17,-30:04:33	1600 ± 3	1.4 ± 0.4	Y	Kern et al. (2008)
GEMS_N5044_7	13:10:59,-15:20:44	2828 ± 8	8.5 ± 1.3	N	...
[MMB2004] J1320-1427	13:20:14,-14:25:41	2748 ± 2	9.7 ± 1.1	Y	McKay et al. (2004)
GEMS_N5044_18	13:11:36,-14:40:40	2488 ± 4	6.3 ± 0.9	Y	Kern et al. (2008)
GEMS_N7714_7	23:45:19,+03:41:28	2755 ± 7	86.0 ± 4.8	N	...
ATCA_1134-37	11:34:02,-37:14:15	3141 ± 5	2.4 ± 0.6^1	Y	Kilborn et al. (2006)

¹ Parameters from ATCA observations.

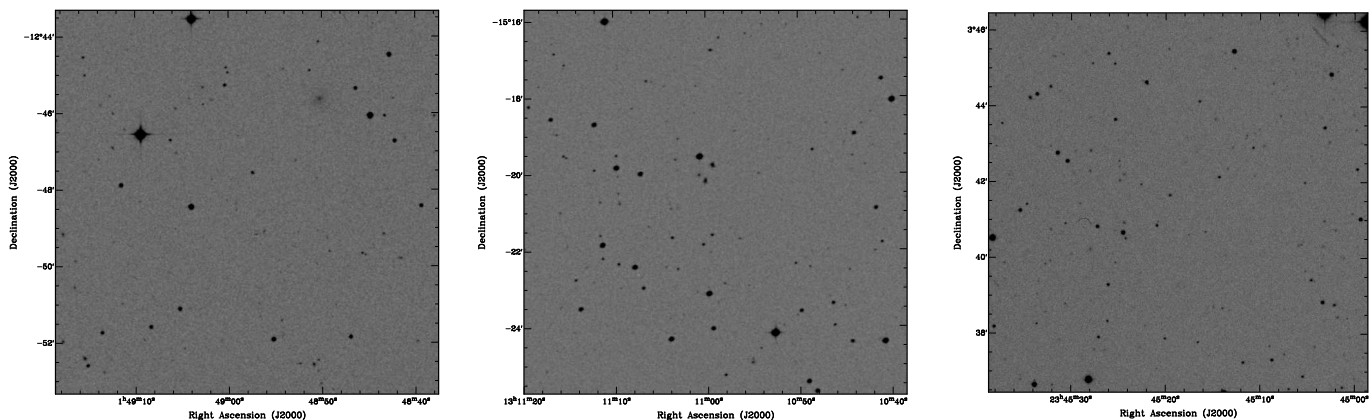


Figure 1. A 10×10 arcminute optical DSSII (R-band) image centred on the Parkes position of the new galaxies in the GEMS HI survey without ATCA follow-up. From left to right they are: GEMS_N720_6, GEMS_N5044_7, GEMS_N7714_7.

amount to the total HI mass of the groups. In general, the previously uncatalogued HI sources correspond to faint dwarf galaxies. The exception is GEMS_N3783_2, for which, despite deep optical imaging and an accurate position from ATCA observations, we are unable to find an optical counterpart for. This detection is discussed in detail in Kilborn et al. (2006).

We determined a redshift for the first time for sixteen previously catalogued galaxies. We have obtained ATCA observations for 12 of these galaxies confirming the optical counterpart. Included in these 12 detections are several instances where there was more than one possible optical counterpart to the original Parkes source, which turned out to comprise two or more galaxies containing neutral hydrogen. Galaxies with newly determined redshifts are listed in Appendix B, along with a reference to the ATCA maps and description of the galaxies where available.

3 HI DISTRIBUTION OF THE GROUPS

Figures 2, 3, 4 and 5 show the integrated HI distribution as measured with the Parkes 64-m telescope for each

of the 16 groups, divided by group X-ray properties. The HI distribution of the groups is varied, from HI being detected throughout the group, to HI only being detected in the outer regions of the group. As we have no distance information for galaxies in the data, these HI maps include the full velocity range of the HI data. In some cases it is likely that the foreground or background HI emission will appear to be part of the group.

3.1 Comparison with X-ray emission

Looking at the HI content and distribution of groups with varying X-ray properties can tell us about the evolutionary stage of the group. We might expect those groups with extended X-ray halos to contain the least HI in them, as is often found in the more dense cluster environment (e.g. Solanes et al. 2001; Cayatte et al. 1990). In some of the groups with extended X-ray emission (see Figures 2 and 3) we do see that there is a lack of HI in the group (e.g. NGC 1407, NGC 4636), however this trend is not so obvious in other groups with extended X-ray emission (e.g. NGC 3783, IC 1459). Looking at the groups where X-rays were only detected in the central galaxy (Figure 4), once again the HI

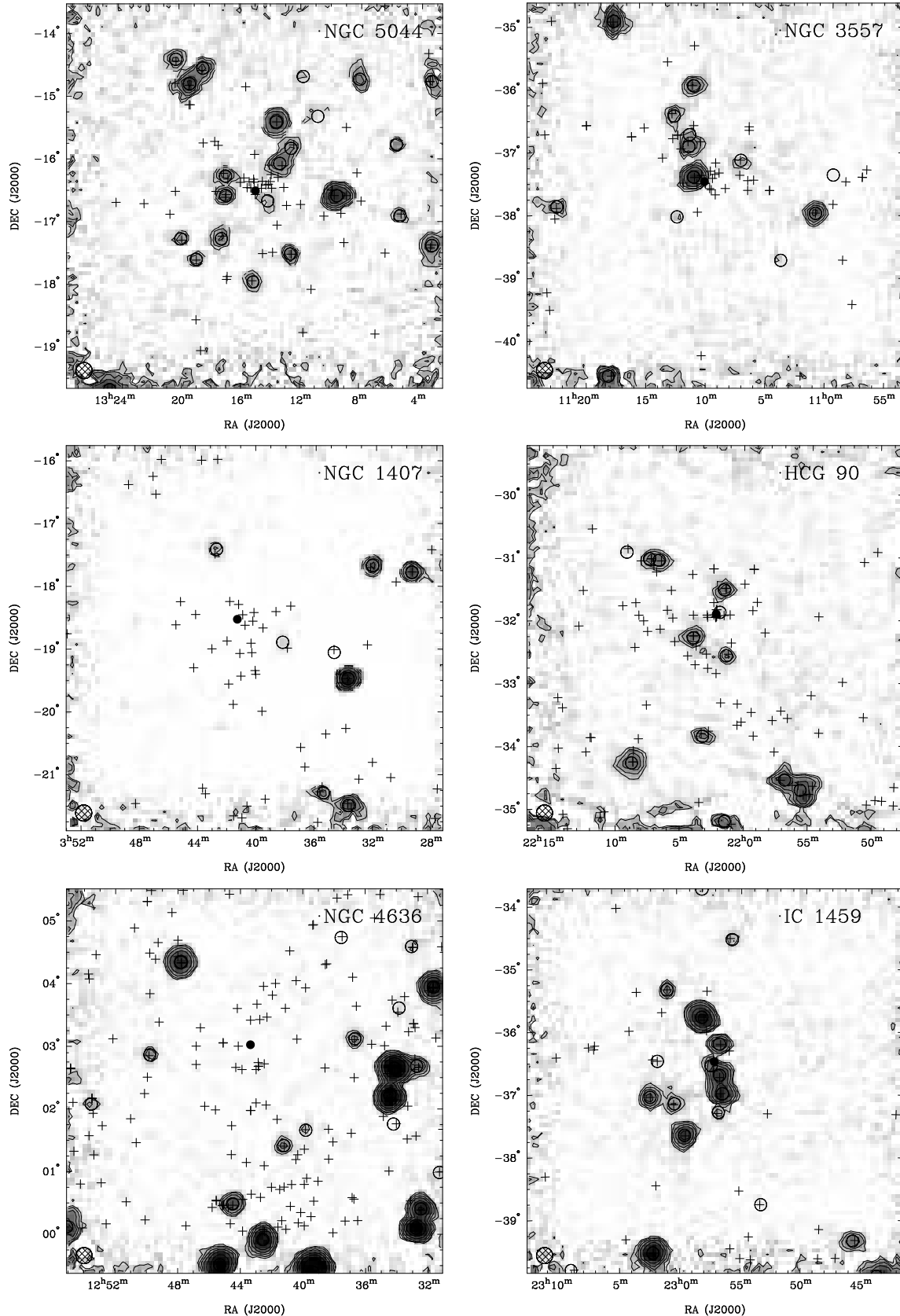


Figure 2. Groups with diffuse group-scale X-ray emission. The contours and greyscale represent the HI intensity, where the contour levels are 1, 2, 4, 8, 16, 32 Jy beam^{-1} , apart from NGC 3783 where the contour levels start at 2 Jy beam^{-1} . Open circles mark the position of the sources we detected in HI, and the crosses show the position of previously catalogued galaxies in NED or the 6dFGS with known velocity in the region of the HI cube. The solid circle marks the luminosity weighted centre for each group (Brough et al. 2006b). The Parkes 15.5' beam is shown in the bottom left hand corner of each image. The images are plotted in order of descending

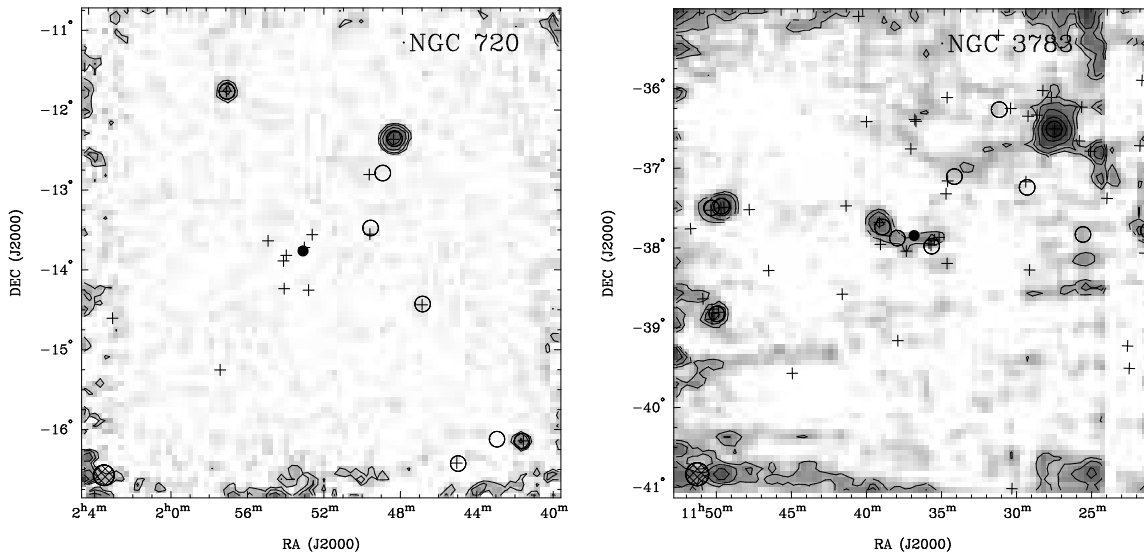


Figure 3. Groups with diffuse X-ray emission. The contour levels and symbols are the same as in Figure 2.

distribution is varied. None of the galaxies in the central region of the NGC 524 group were detected in HI but in other groups such as NGC 1052 and NGC 1566, the majority of galaxies were detected. The two groups without detected X-rays shown in Figure 5 do not present a consistent picture in HI emission, with few galaxies detected in the NGC 7714 group, and most galaxies detected in HI in the NGC 1808 group.

To obtain a quantitative comparison of the HI content of the groups compared to X-ray properties of the groups we look at the HI mass detected in the groups. We determine the total HI mass, and the HI contained within r_{500} for the groups. r_{500} is the radius corresponding to an overdensity of 500 times the critical density, and is used in Osmond & Ponman (2004) and Brough et al. (2006b) for analysis of GEMS groups. Here and in subsequent analysis of the groups, we refer specifically to the members of the groups defined by the friends-of-friends algorithm in Paper I (Brough et al. 2006b). We use the Kendall’s rank correlation probabilities for each group parameter pair, using the IRAF/STSDAS/STATISTICS package routine, as was used in Brough et al. (2006b). As explained in Brough et al. (2006b), Kendall’s rank correlation is more reliable for samples where $N < 30$ than the Spearman rank correlation, and it is non-parametric. Where available we use upper limits for X-ray luminosities, and HI masses, and the survival analysis tasks available in IRAF take these into account in the correlation. We also use the IRAF Buckley-James algorithm to fit straight lines to our data.

Figure 6 shows the group HI mass (within r_{500}), and the normalised HI mass ($M_{HI,tot}/N_{gals}$) plotted against the X-ray properties (X-ray extent, L_X and T_X) of the groups. No significant correlation is seen between the extent of the group X-ray emission and the group HI mass, or between the X-ray luminosity and total group HI mass. A trend is seen however between the group HI mass and the X-ray temperature, with a probability of 87.8%, calculated using the Kendall’s Tau method described above. Fitting a straight

line to these points using the Buckley-James algorithm gives the functional fit of

$$T_X = -0.18^{\pm 0.14} M_{HI,r500} + 2.4 \quad (1)$$

with a standard deviation on the regression of 0.28.

Using the group HI mass within r_{500} to compare with X-ray properties is prone to bias due to the low number statistics in individual groups. For example, just one gas-rich galaxy can make a group appear to be gas-rich, when in fact the majority of the galaxies in the group are gas-poor. To better understand the global HI content of a group, we have determined the *normalised group HI mass*, which is the *total* HI mass in the group divided by the total number of group members.

When using this quantity, we again find no correlation between the group X-ray extent and the normalised group HI mass, however a weak trend is seen between the X-ray luminosity and the normalised group HI mass with a probability of 80%, and a stronger trend between the X-ray temperature and normalised group HI mass with a probability of 93% (Figure 6). The Buckley-James fit to the X-ray luminosity and temperature is

$$L_X = -0.54^{\pm 0.3} M_{HI,tot}/N_{gal} + 44.3 \quad (2)$$

with a standard deviation on the regression of 0.7, and

$$T_X = -0.2^{\pm 0.12} M_{HI,tot}/N_{gal} + 2.3 \quad (3)$$

with a standard deviation on the regression of 0.26. Using the normalised group HI mass in comparison to the X-ray properties of a group have shown that the presence of an extended intra-group medium and the depth of the potential well as indicated by the X-ray temperature of the group is more important to the HI content of galaxies in groups, than the physical extent of the hot intra-group medium.

3.2 Dependence on total mass and morphology

We examined the relationships between the total HI mass of the groups, and their respective virial mass and velocity dis-

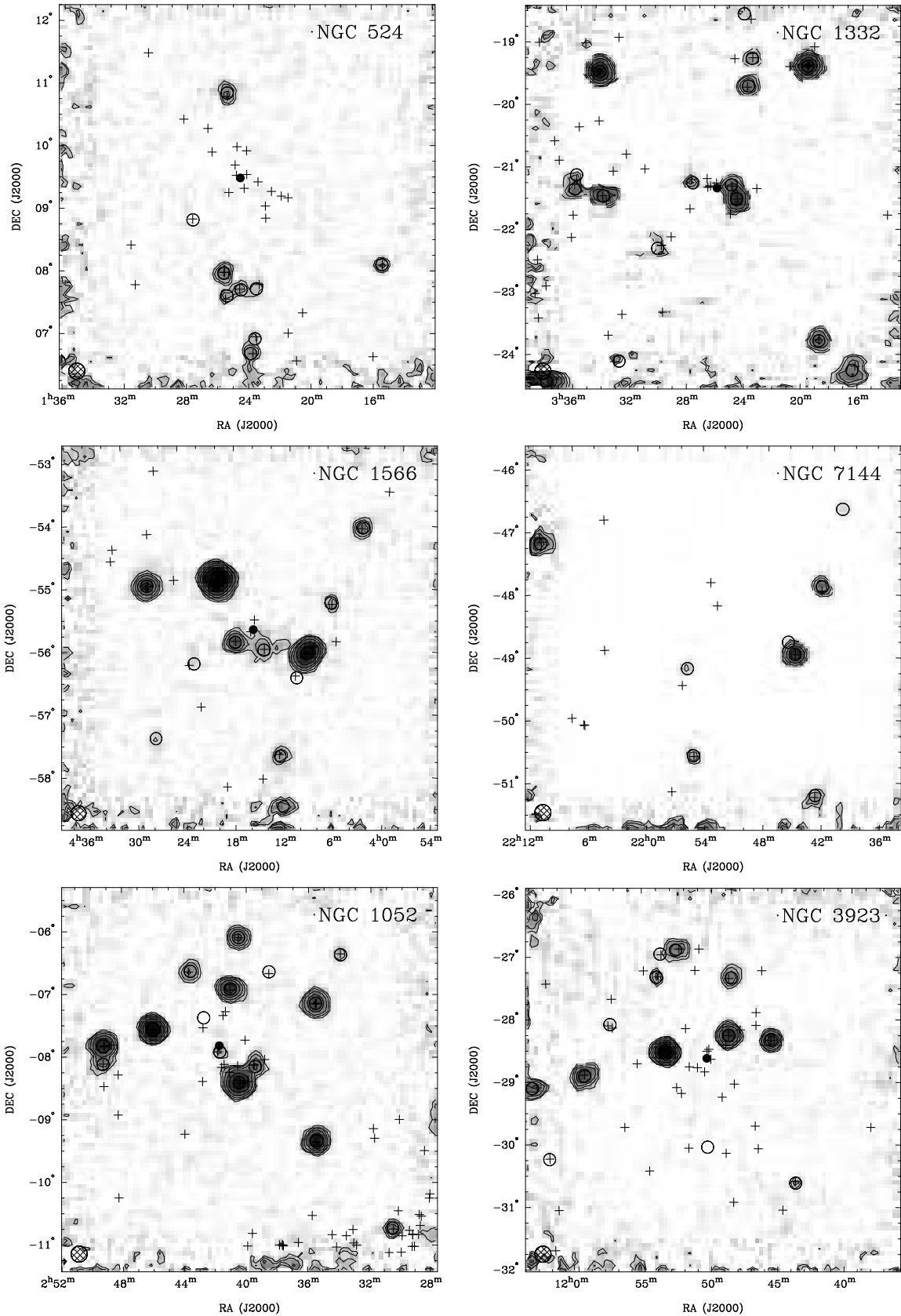


Figure 4. Groups with central galaxy only X-ray emission. The contour levels and symbols are the same as in Figure 2.

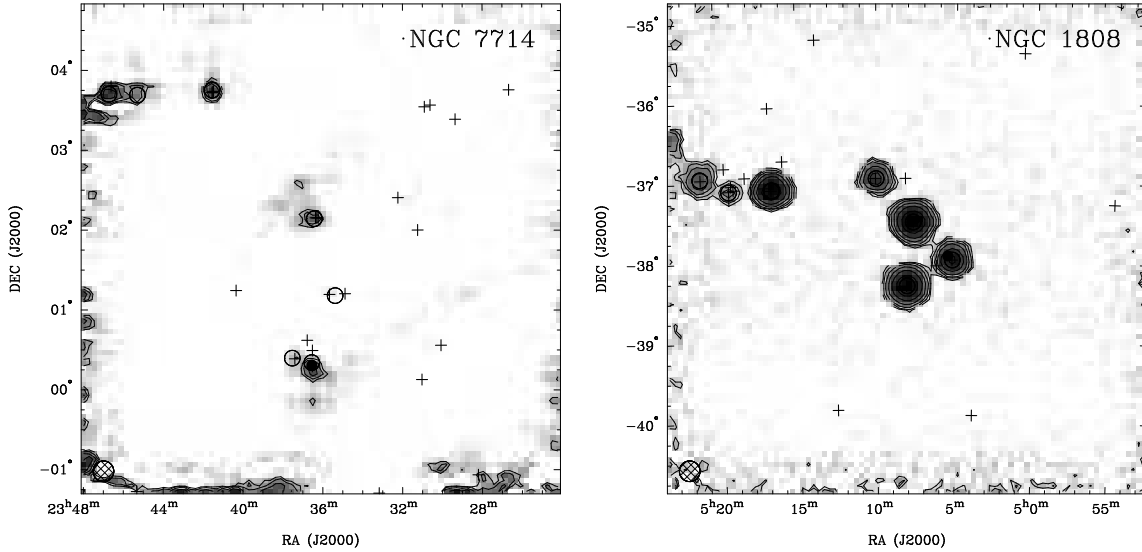


Figure 5. Groups undetected in X-rays. The contour levels are 1, 2, 4, 8, 16, 32 Jy beam^{-1} , apart from NGC 7714, where the contour levels start at 2 Jy beam^{-1} . The symbols are the same as in Figure 2.

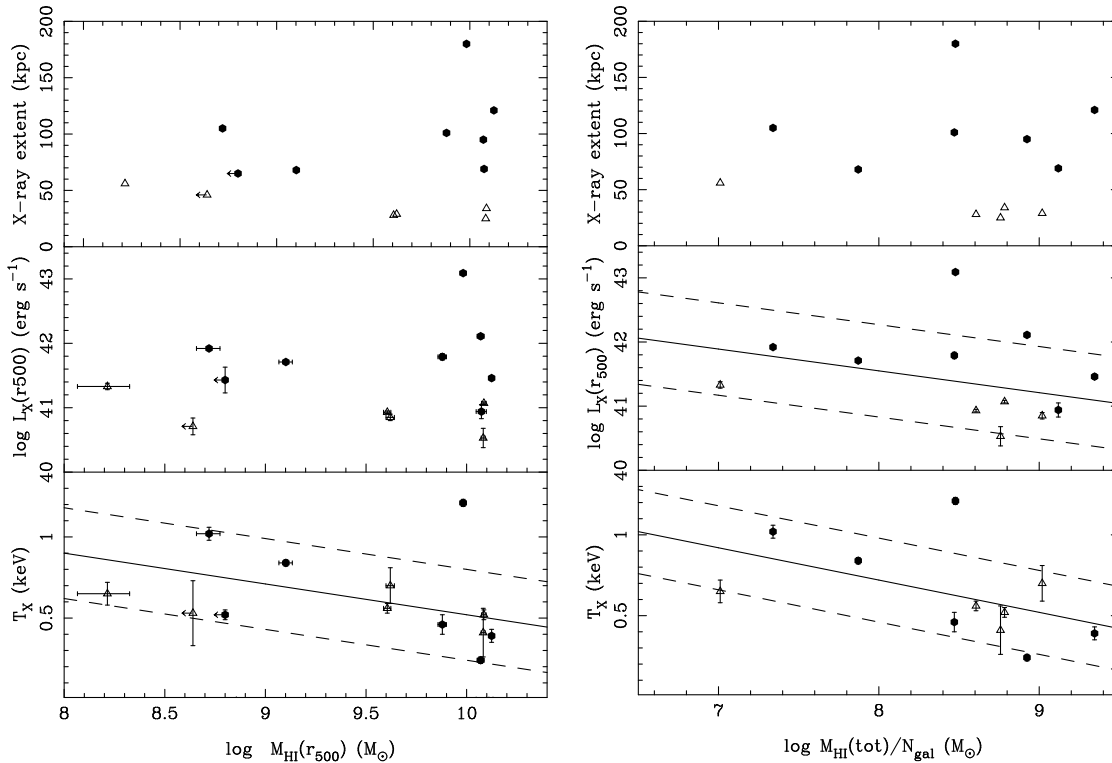


Figure 6. Total group HI mass compared with X-ray properties. Left: The top panel shows the total HI mass of the group (within the r_{500} radius) against the extent of the X-ray emission in the group. The middle (bottom) panel plots the total HI mass of the group against the X-ray luminosity (temperature). Right: The top panel shows the normalised HI mass of the group against the extent of the X-ray emission in the group. The middle (bottom) panel plots the normalised HI mass of the group against the X-ray luminosity (temperature). The solid lines show a Buckley-James regression fit to the data, and the dashed lines show the $1\text{-}\sigma$ standard deviation on the fit. The filled circles are groups with a detected extended X-ray emission, and the triangles are groups with no extended X-rays emission.

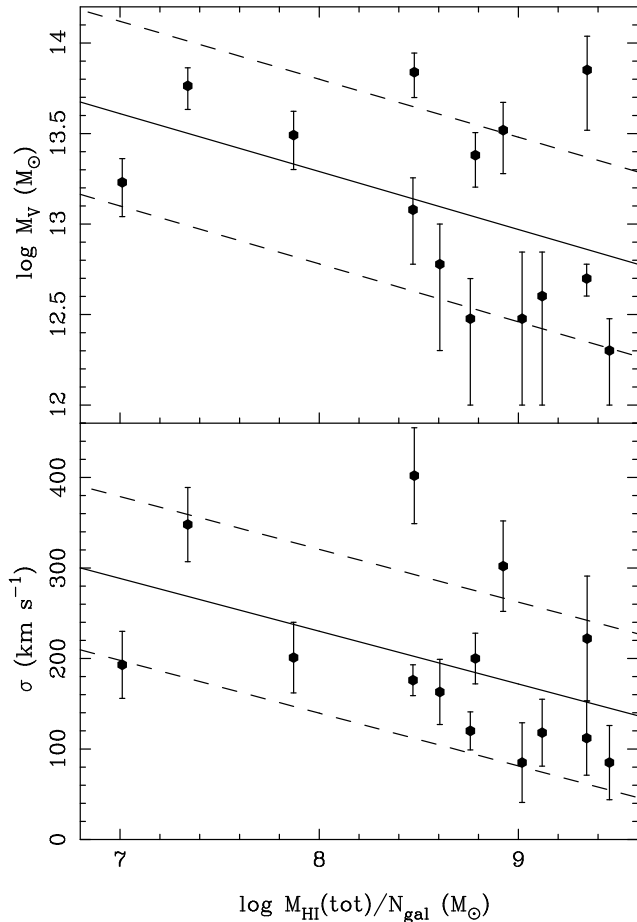


Figure 7. Normalised group H I mass versus the group virial mass (top) and the velocity dispersion of group (bottom). The solid lines show a Buckley-James regression fit to the data, and the dashed lines show the standard deviation on the fit.

persion. We found no correlation in these parameters. However, when we compared the normalised H I group mass with these parameters, we did find trends within the data. Figure 7 shows the corresponding trends. Using the Kendall’s Tau statistic, we found that the probability there was a correlation between the group virial mass and the normalised H I mass was 81.2%, with a Buckley-James regression of

$$M_V = -0.32^{\pm 0.19} M_{HI,tot}/N_{gal} + 15.8, \quad (4)$$

with a standard deviation on the regression of 0.5. There was a stronger correlation between the normalised H I mass of the groups and the velocity dispersion of 95.2%, with a Buckley-James regression of

$$\sigma_v = -58.3^{\pm 33.9} M_{HI,tot}/N_{gal} + 696.5, \quad (5)$$

with a standard deviation on the regression of 90.5. These results compare well with the finding of a trend between the normalised H I mass and the X-ray temperature and luminosity, as these quantities all relate to how evolved a group is, and the depth of the potential well.

We also looked for a correlation between the total K-band luminosity and the total H I group mass and normalised H I group mass, however we found none.

It is well known that the H I content of galaxies depends on if they are early or late-type, with later types tending to

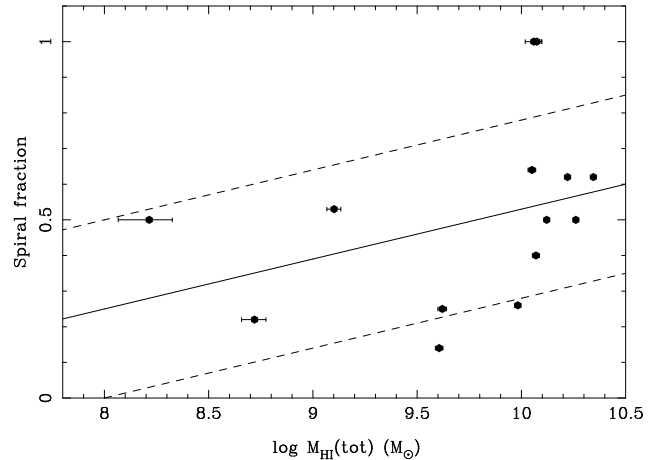


Figure 8. Total group H I versus group spiral fraction. The solid lines show a Buckley-James regression fit to the data, and the dashed lines show the standard deviation on the fit. A trend is seen for groups with a higher spiral fraction to be more H I rich.

be the more H I-rich. Figure 8 shows the total group H I mass plotted against the group spiral fraction. There is a 92.3% probability that the two parameter sets are correlated, with a Buckley-James regression of

$$F_{sp} = 0.14^{\pm 0.11} M_{HI,tot} - 0.87, \quad (6)$$

with a standard deviation on the regression of 0.25. There was a weaker trend (81% probability) between the normalised H I group mass and the spiral fraction of the groups. This result is as expected, showing that the groups with a higher spiral fraction also contain the most neutral hydrogen, although the relationship does show some considerable scatter.

Using the normalised group H I mass, we have shown that the H I content of groups is dependent on the X-ray temperature, and to a lesser extent the X-ray luminosity. However, physical size of the X-ray emission region does not have any effect on the the H I content of the groups. There was a strong trend such that the normalised H I content of groups was lower for groups with a higher velocity dispersion. Groups with a higher spiral fraction contained more H I. These results show a consistent picture, that the more evolved groups, that have lower spiral fractions, higher velocity dispersions and higher X-ray temperatures also contain the least neutral hydrogen per group member.

4 H I CONTENT OF GALAXIES IN GROUPS

As we have seen in Figure 8, the H I content of groups is dependent on the make-up of their morphological types. To further investigate the processes that are occurring in the group environment, we now consider the H I content of the individual galaxies, and compare them to similar galaxies in the non-group (i.e. ‘field’) environment.

We investigate whether the galaxies in groups are undergoing transformations, by looking at their relative H I content. We determine the ‘expected’ H I from the optical properties of a galaxy, and compare it with the detected H I emission from our survey. To compare the two

values, we determine an ‘HI deficiency parameter’, Def (Haynes & Giovanelli 1984), which is the difference between the expected HI mass and the observed HI mass:

$$Def = \log M_{HI}(expected) - \log M_{HI}(obs). \quad (7)$$

We calculate the expected HI for a galaxy using its optical properties, ie optical diameter, and morphological type. We obtained morphological types and optical diameters for our group galaxies from the LEDA¹ database. The relationships we used to calculate the expected HI content are from Kilborn et al. (2005), which also uses the LEDA database for optical parameters. There is a large scatter in the relationship for early type galaxies, so we limit our investigation to spiral galaxies of type Sa and later. Due to the large beam-size of the Parkes telescope ($\sim 15'$), there are a number of HI sources with uncertain optical counterparts. For the HI deficiency analysis, we only include galaxies that have one single optically matched counterpart at the same redshift as the source. It is possible that we will still include multiple galaxies in our analysis, with galaxies of unknown redshift in the Parkes beam. This will have the effect of making a particular galaxy appear more HI rich than it actually is.

Figure 9 shows the HI deficiency of non interacting galaxies in our sample with available optical data as described above, versus their projected distance from the group centre. We consider galaxies with $Def > 0.3$ to be HI deficient (i.e. they contain less than half HI as expected). Overall, there is no average trend for galaxies to be more HI deficient in the centres of groups. However, those galaxies that are HI deficient tend to lie closer to the centre of the groups rather than on the edges.

Figure 10 shows the HI deficiency of galaxies versus their projected distance from the group centre, normalised by the virial radius of the group. This shows that almost half of the HI deficient galaxies lie 3 - 4 virial radii from the group centre, whilst the others lie within 2 virial radii of the group centre.

Figure 11 shows the proportion of HI deficient galaxies compared to the number of group members (with HI deficiency measurement available), versus the X-ray luminosity of the group. For comparison, these quantities are also plotted for clusters, taken from Giovanelli & Haynes (1985). We find no correlation between X-ray luminosity and the fraction of HI deficient spirals. Contrary to our results, Giovanelli & Haynes (1985) find an apparent trend between the HI deficient fraction of clusters and the X-ray luminosity, however with a larger sample Solanes et al. (2001) found no clear trend.

Figure 12 shows the HI deficient fraction of galaxies compared to the group velocity dispersion. No correlation is seen between these two parameters, as might have been expected if the HI deficiencies seen in groups are due to ram pressure stripping.

4.1 Removal of gas from galaxies in groups

We have found that some galaxies in the group environment display an HI deficiency. What is the mechanism for the removal of the gas from these galaxies,

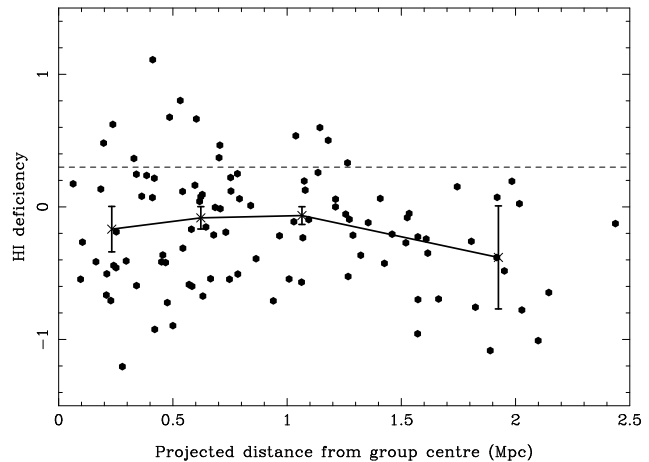


Figure 9. HI deficiency versus distance from group centre. Galaxies that are HI deficient have a positive value for the HI deficiency parameter. The crosses indicate the mean HI deficiency, with equal numbers of galaxies in each bin, whilst the error bars show the standard error on this mean value. Points above the dashed line are defined as HI deficient, containing less than half of the HI mass expected.

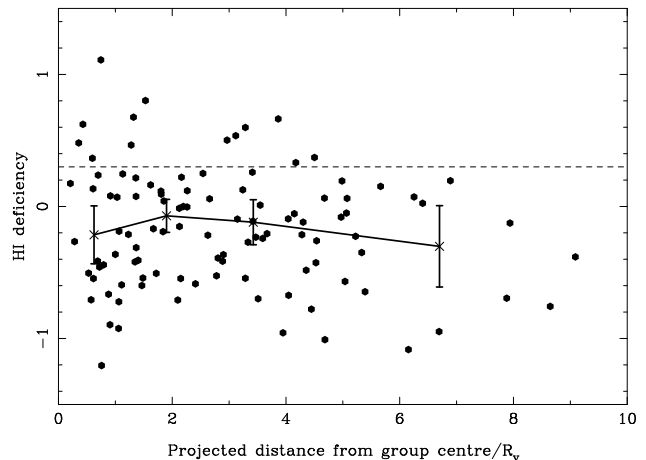


Figure 10. HI deficiency versus distance from group centre, in units of virial radii. Galaxies that are HI deficient have a positive value for the HI deficiency parameter. The crosses indicate the mean HI deficiency, with equal numbers of galaxies in each bin, whilst the error bars show the standard error on this mean value. Points above the dashed line are defined as HI deficient, containing less than half of the HI mass expected.

and what effect does gas removal have on the galaxy itself? Previous studies have found that galaxy interactions, and tidal stripping are the dominant mechanism in loose groups, as the HI deficiency of galaxies appears to increase with galaxy density, and is inversely correlated with radial velocity (Omar & Dwarakanath 2005), and HI deficient galaxies are found in groups without an intragroup medium (Kilborn et al. 2005). In compact groups, the stripping mechanism is not so clear, as the most HI-deficient groups tend to show intragroup X-ray emission (Verdes-Montenegro et al. 2001).

The group we found that had the highest number of HI deficient galaxies is NGC 4636 - a dynamically evolved

¹ <http://leda.univ-lyon1.fr/>

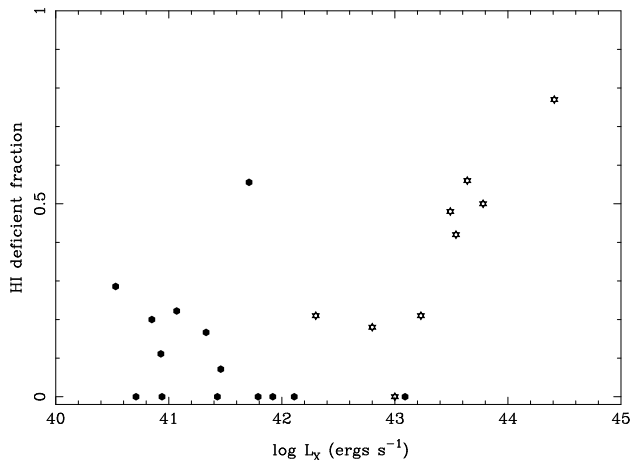


Figure 11. HI deficient fraction versus X-ray luminosity. The filled circles represent the fraction of HI deficient galaxies in the GEMS groups, and the stars show this for clusters (Giovanelli & Haynes 1985).

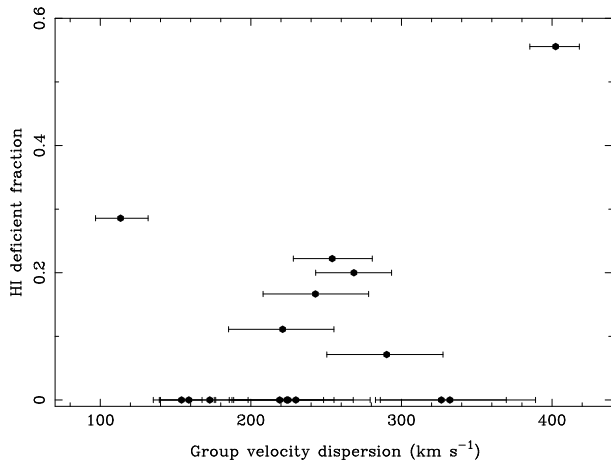


Figure 12. HI deficient fraction versus group velocity dispersion.

group, which lies on the outskirts of the Virgo cluster. However, most of the other HI deficient galaxies in our groups lie in groups that do not have a hot intra-group medium, and thus ram pressure stripping cannot be attributed to the gas-loss from the galaxies in these groups.

While a hot IGM does not seem to make a difference to the gas-loss of galaxies in groups, the position in the group does - we find that two thirds of the HI deficient galaxies lie within 1 Mpc projected distance of the group centre (see Figure 9), although not every HI deficient galaxy is classified as a member of the group.

Our results are consistent with the scenario that the dominant mechanism of gas removal in the group environment is via tidal stripping through galaxy-galaxy or galaxy-group interactions, rather than ram pressure stripping, although we note that the group with the most HI deficient members also has the highest velocity dispersion.

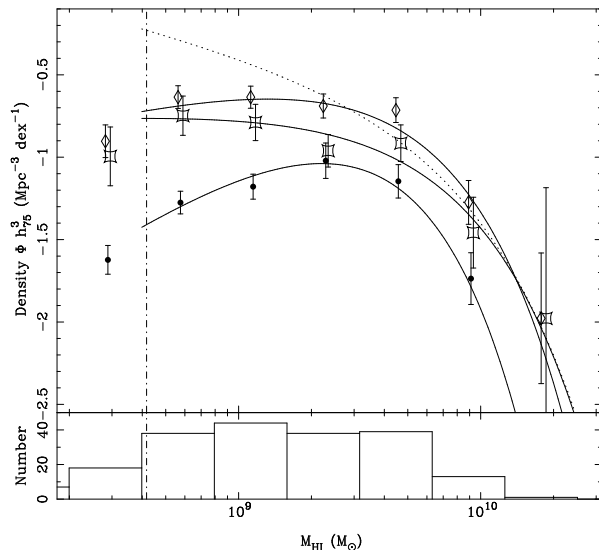


Figure 13. HI mass function for the composite group. The open diamonds show the HI mass function for all galaxies we detected in the HI cubes, the filled circles are for galaxies determined to be members of groups, and the open squares are the galaxies that are not members of the groups. The solid lines show a least-squares fit of a Schechter function to the binned data, and the dashed line is the HI mass function from HIPASS for comparison (Zwaan et al. 2005). The histogram shows the HI distribution of all detected galaxies. The Schechter fit parameters are listed in Table 4. The errors on each point are statistical errors.

5 HI MASS FUNCTION IN GROUPS

To investigate the distribution of HI mass in groups, we construct an HI mass function, to compare the HI content of our groups to that of the field.

Due to the low number statistics for the individual groups, we combine the data from each group together to determine a composite HI mass function for the groups. We normalised the number of galaxies in each HI cube by the available volume in the HI cube according to the redshift range covered by the cube.

Figure 13 shows the resulting HI mass function for the composite group. We show the HI mass function for the full sample, one for those galaxies found in the groups according to Brough et al. (2006b), and the HI mass function for galaxies found in the HI cubes, but not in the groups.

To parameterise our data, we fit a Schechter function (Schechter 1976) to each data set:

$$\Psi\left(\frac{M_{HI}}{M^*}\right)d\left(\frac{M_{HI}}{M^*}\right) = \theta^* \left(\frac{M_{HI}}{M^*}\right)^{-\alpha} \times \exp\left(-\frac{M_{HI}}{M^*}\right)d\left(\frac{M_{HI}}{M^*}\right) \quad (8)$$

where M^* is the characteristic HI mass, α is the low-mass slope, and θ^* is the normalisation of the mass function. The solid lines show least-square fits of a Schechter function to the binned data. We do not fit for data below the completeness limit of the least sensitive group observations, at an HI mass of $5 \times 10^8 M_\odot$.

We show the Zwaan et al. (2005) HI mass function from HIPASS for comparison (normalised to our data), with $\log M^* = 9.8 M_\odot$, and $\alpha = 1.37$. Schechter parameters found for the group and non-group galaxies are summarised in Table 4.

We find that the overall HI mass function in the gen-

Table 4. HI mass function Schechter parameters. Values for the low-mass slope of the HI mass function, α , and the characteristic HI mass, M^* for group, non-group and all detected galaxies, and HIPASS for comparison (Zwaan et al. 2005).

Sample	α	$\log M^* M_\odot$
All sample	0.65 ± 0.17	9.6 ± 0.1
Group galaxies	0.0 ± 0.18	9.7 ± 0.2
Non-group galaxies	0.92 ± 0.23	9.4 ± 0.06
HIPASS	1.37 ± 0.03	9.8 ± 0.03

eral group environment (i.e. the groups, and galaxies surrounding the groups) is very flat, with a low-mass slope of $\alpha = 0.65 \pm 0.17$. When the sample is divided into galaxies that are members of the groups, and those that are not, we find a noticeable difference in the shape of the HI mass function. For those galaxies that are confirmed members of a group, the HI mass function shows a very shallow low-mass slope ($\alpha = 0.0 \pm 0.18$). We find a steeper slope for those galaxies surrounding the groups ($\alpha = 0.92 \pm 0.23$), which is closer to, but still significantly shallower than, the global result from Zwaan et al. (2005) of $\alpha = 1.37$, perhaps indicating that group processes may apply to galaxies nearby groups as well.

Galaxies of low HI mass could be dwarf galaxies, early-type galaxies (which typically contain less HI than spiral galaxies), or gas-deficient spiral galaxies. The group HI mass function also shows, that the highest HI mass galaxies are not group members, with the highest HI mass being in the $\log M_{HI} = 9.75 M_\odot$ bin. So not only are the least massive galaxies found in fewer numbers in the group environment, but we also do not find the most massive galaxies either. This may be an effect of stripping of the most gas-rich galaxies in the group environment, similar as is seen in the Coma cluster (Gavazzi et al. 2006).

Our results on the HI mass function for groups show similarity to that of the Virgo cluster, which is found to peak at an HI mass of $\sim 4 \times 10^8 M_\odot$, and decline thereafter (Davies et al. 2004; Gavazzi et al. 2005). Gavazzi et al. (2005) used a Monte Carlo simulation to model the effect of HI deficiency on the shape of the HI mass function for the Virgo cluster. They found a good agreement between their simulations and the HI mass function, showing that it is possible to transform the field HI mass function into that seen in a cluster by galaxies losing their neutral hydrogen content. Our result of finding HI deficient galaxies in groups, combined with the observation of a flat HI mass function in groups suggests a similar process could be occurring in groups.

6 DISCUSSION

The group environment appears to play an important part in transforming galaxies in the local universe, with many of the processes seen in the much denser cluster environment also apparent in the less extreme group environment. This includes the removal of gas from spiral galaxies, the discovery of X-ray halos in galaxy groups indicating a deep potential well and the virialisation of galaxy groups.

When comparing the HI content of galaxy groups to

the X-ray properties of the groups, we found that the groups with the highest X-ray temperatures and luminosities typically contained less neutral hydrogen. These results were strengthened when we examined the normalised HI content of the groups, where the HI content was normalised by the number of group members. We also found that the groups with the highest virial masses and velocity dispersions also contained less HI. These results are consistent with the picture that groups lose their HI as they become more evolved, grow their potential wells and increase in X-ray brightness, and also increase in virial mass and velocity dispersion. However, these results do not prove that the group environment has caused the galaxies to contain less HI - to investigate this question, we looked at the HI deficiency of galaxies within the group environment, compared to a much larger field sample.

We found that a number of the galaxies in our sample were HI deficient. About two-thirds of the HI deficient galaxies lie within a projected distance of 1 Mpc from the group centre. This is consistent with previous results for the cluster environment (Solanes et al. 2001), although the percentage of HI deficient galaxies found in the loose groups is much lower than that seen in clusters. While we observe HI deficient galaxies within the centres of X-ray bright groups, they are also present in groups that have no detected intra-group medium. Thus the mechanism for this HI deficiency is not clear - in the case where no IGM is present, ram pressure stripping cannot be the cause of the HI deficiency, and the loss of gas is more easily explained by tidal stripping. Our high resolution images of interacting galaxies in groups (see Kern et al. 2008) show that HI can be removed from galaxies in interactions and mergers, although the ultimate fate of the gas (whether it is lost to the IGM, or falls back onto one or both of the galaxies) is not certain. Gomez et al. (2003) find there is a ‘break’ in the star-formation-density relationship for clusters and groups at a density of $\sim 1 h_{75}^{-2} \text{Mpc}^{-2}$, which corresponds to clustercentric radius of 3–4 virial radii. This corresponds to the maximum radius we find HI deficient galaxies in our groups, perhaps indicating a correlation between the loss of gas of galaxies in dense environments, and the decrease in their star-formation rate. This suggests a pre-processing in the group environment.

Comparing the HI mass function from our combined groups sample with previous studies, we find that the low-mass slope is flatter than found in HIPASS, with a low-mass slope of 0.0 ± 0.18 , compared with the field HIPASS low-mass slope of $\alpha = 1.37$ (Zwaan et al. 2005). Our result goes against the trend found by Zwaan et al. (2005) for a steeper low-mass slope in denser regions, but is more consistent with the result of Springob, Haynes & Giovanelli (2005) and Rosenberg & Schneider (2002) who find tentative evidence for flattening of the low-mass slope in denser environments, and Freeland et al. (2009) who find a flat low-mass slope in groups.

Our HI results show that the evolutionary status of the group, and the morphological make-up are important in determining the HI content of a group. This result is consistent with Giovanelli & Haynes (1985), who find in a study of the HI content of clusters, those clusters that are not detected in X-rays, and that contain a higher proportion of spiral galaxies, are not HI deficient.

7 CONCLUSIONS

We have investigated the evolution of galaxies in loose groups through an H I and X-ray survey of 16 groups. We find that the X-ray emission and H I content of the groups is not simply correlated, and that while some groups that show extended X-ray emission have little H I content, others are H I rich. We find the total H I content is anti-correlated with the X-ray temperature, and to a lesser extent the X-ray luminosity, and similarly the H I content was correlated with the velocity dispersion or virial mass of the group. Not surprisingly, groups with a higher fraction of spirals also contained the most H I. These results indicate that those groups that are more evolved contain less H I than younger groups. We determined the H I deficiency of galaxies within the groups, and found that around two thirds of H I deficient galaxies were preferentially located at a projected distance of less than 1 Mpc from the group centre. There was no correlation found between the fraction of H I deficient galaxies in a group and the X-ray luminosity. We calculated a combined H I mass function for the groups, and found that it is very shallow compared to the global HIPASS H I mass function.

ACKNOWLEDGMENTS

We thank Ruth Musgrave for help with searching the Parkes H I cubes, and Nuria McKay for helping with the Parkes observations. We thank the staff at the Parkes and Narrabri observatories for their help in the project. We acknowledge the expertise of Mark Calabretta, and thank him for his assistance with AIPS++.

REFERENCES

- Banks G. D., Disney M. J., Knezek P.M. et al. 1999, *ApJ*, 524, 612
- Barnes D. G., de Blok W. J. G., 2001, *AJ*, 122, 825
- Barnes D. G., Staveley-Smith L., de Blok W. J. G. et al. 2001, *MNRAS*, 322, 486
- Brough S., Forbes D. A., Kilborn V. A., Couch W., Colless M., 2006a, *MNRAS*, 369, 1351
- Brough S., Forbes D. A., Kilborn V. A., Couch W., 2006b, *MNRAS*, 370, 1223
- Butcher H., Oemler A. Jr. 1978, *ApJ*, 219, 18
- Cayatte V., van Gorkum J. H., Balkowski C., Kotanyi C., 1990, *AJ*, 100, 604
- Chamaraux P., Masnou J., 2004, *MNRAS*, 347, 541
- Davies J., Minchin R., Sabatini S. et al., 2004, *MNRAS*, 349, 922
- Eke V. R., Baugh C. M., Cole S. et al. 2004, *MNRAS*, 348, 866
- Forbes D. A., Ponman T., Pearce F. et al., 2006, *PASA*, 23, 38
- Freeland E., Stilp A., Wilcots E. 2009, *AJ*, in press
- Gavazzi G., Boselli A., van Driel W., O’Neil K. 2005, *A&A*, 429, 439
- Gavazzi G., O’Neil K., Boselli A., van Driel W. 2006, *A&A*, 449, 929
- Giovanelli R., Haynes M. P. 1985, *ApJ*, 292, 404
- Gomez P. L., Nichol R. C., Miller C. J. et al. 2003, *ApJ*, 584, 210
- Haynes M. P., Giovanelli R. 1984, *AJ*, 89, 758
- Jones D. H., Saunders W., Read M., Colless M., 2005, *PASA*, 22, 277
- Kern K. M., Kilborn V. A., Forbes D. A., Koribalski B. 2008, *MNRAS*, 384, 305
- Kilborn V. A., Koribalski B. S., Forbes D. A., Barnes D. G., Musgrave R. C., 2005, *MNRAS*, 356, 77
- Kilborn V. A., Forbes D. A., Koribalski B. S., Brough S., Kern K., 2006, *MNRAS* 371, 739
- Kovac K., Oosterloo T. A., van der Hulst J. M. 2005, in "Near-field Cosmology with Dwarf Elliptical Galaxies", Proceedings IAU Colloquium No. 198, B. Bingelli & H. Jerjen eds, p351
- Lewis I., Balogh M., De Propriis R. et al. 2002, *MNRAS*, 334, 673
- Magri C., Haynes M. P., Forman W., Jones C., Giovanelli R. 1988, *ApJ*, 333, 136
- McKay N. P. F., Mundell C. G., Brough S. et al., 2004, *MNRAS*, 352, 1121
- Meyer M. J., Zwaan M. A., Webster R. L. et al., 2004, *MNRAS*, 350, 1195
- Mulchaey J. S., Zabludoff A. I. 1998, *ApJ*, 496, 73
- Omar A., Dwarakanath K. S., 2005, *JApA*, 26, 1
- Osmond J. P. F., Ponman T. J., 2004, *MNRAS*, 350, 1511
- Rasmussen J., Ponman T. J., Mulchaey J. S., 2006, *MNRAS*, 370, 453
- Rosenberg J. L., Schneider S. E. 2002, *ApJ*, 567, 247
- Schechter P. 1976, *ApJ*, 203, 297
- Sengupta C., Balasubramanyam R., 2006, *MNRAS*, 369, 360
- Sengupta C., Balasubramanyam R., Dwarakanath K. S. 2007, *MNRAS*, 378, 137
- Solanes J. M., Manrique A., Garcia-Gomez C., Giovanelli R., Haynes M. P., 2001, *ApJ*, 548, 97
- Springob C. M., Haynes M. P., Giovanelli R., 2005, *ApJ*, 621, 215
- Verdes-Montenegro L., Yun M. S., Williams B. A., Huchtmeier W. K., Del Olmo A., Perea J. 2001, *A&A*, 377, 812
- Wilman D. J., Oemler A., Mulchaey J. S., McGee S. L., Balogh M. L., Bower R. G. 2009, *ApJ*, 692, 298
- Zwaan M. A., Meyer M. J., Staveley-Smith L., Webster R. L., 2005, *MNRAS*, 359, L30

Appendices

APPENDIX A: H I PARAMETERS FOR ALL GEMS H I DETECTIONS.

APPENDIX B: OPTICAL COUNTERPARTS TO THE H I DETECTIONS.

This paper has been typeset from a $\text{T}_{\text{E}}\text{X}/\text{L}^{\text{A}}\text{T}_{\text{E}}\text{X}$ file prepared by the author.

Table A1. H I detections of the galaxies in groups. The columns are as follows: (1)GEMS H I catalogue designation; (2) α (J2000) [h m s];(3) δ (J2000)[$^{\circ}$ $''$]; (4) Systemic velocity, V_{sys} , of source in km s^{-1} ; (5) error on V_{sys} , in km s^{-1} ; (6) H I line width of source at 20% of the peak, V_{20} , in km s^{-1} ; (7) error on V_{20} , in km s^{-1} ; (8) H I line width of source at 50% of the peak, V_{50} , in km s^{-1} ; (9) error on V_{50} , in km s^{-1} ; (10) Peak flux, S_p in Jy; (11) error on S_p in Jy; (12) total H I flux, S , in Jy km s^{-1} ; (13) error on S , in Jy km s^{-1} ; (14) H I mass, M_{HI} , assuming group distance as given in Table 2, in units of $10^8 M_{\odot}$; (15) error on M_{HI} , in units of $10^8 M_{\odot}$.

(1)	(2)	(3)	(4)	(5)	(6)	(7)	(8)	(9)	(10)	(11)	(12)	(13)	(14)	(15)
GEMS_N524_1	1:25:36.989	7:58:41.185	2898	3	138	9	56	6	0.113	0.007	8.8	0.68	10.31	0.79
GEMS_N524_2	1:25:24.242	7:36:53.923	2778	3	169	9	145	6	0.054	0.006	5.9	0.63	6.91	0.74
GEMS_N524_3	1:24:29.564	7:42:35.913	2740	2	231	6	211	4	0.064	0.005	8.2	0.61	9.61	0.72
GEMS_N524_4	1:23:35.983	6:55:45.128	2728	2	61	6	44	4	0.051	0.005	2.2	0.35	2.58	0.41
GEMS_N524_5	1:25:24.181	10:51:08.303	2549	3	136	9	96	6	0.082	0.007	6.9	0.63	8.08	0.74
GEMS_N524_6	1:15:25.003	8:06:18.193	2348	2	155	6	144	4	0.056	0.005	5.8	0.52	6.80	0.61
GEMS_N524_7	1:23:52.770	6:41:30.747	2335	1	43	3	34	2	0.121	0.008	4.2	0.49	4.92	0.58
GEMS_N524_8	1:23:30.768	7:43:42.491	2689	3	126	9	104	6	0.039	0.005	2.5	0.40	2.93	0.47
GEMS_N524_9	1:27:36.255	8:49:36.256	2430	4	74	12	61	8	0.029	0.006	1.4	0.41	1.64	0.48
GEMS_N720_1	1:41:40.196	-16:08:58.995	1635	2	120	6	111	4	0.056	0.006	4.2	0.50	6.54	0.78
GEMS_N720_2	1:42:58.502	-16:07:44.993	1154	9	174	27	147	18	0.019	0.006	1.4	0.53	2.18	0.82
GEMS_N720_3	1:46:53.731	-14:26:35.705	1742	5	145	15	71	10	0.047	0.005	3.3	0.46	5.14	0.72
GEMS_N720_4	1:48:22.883	-12:22:30.845	1613	2	108	6	82	4	0.182	0.010	15.0	0.96	23.34	1.49
GEMS_N720_5	1:56:57.619	-11:46:50.562	1865	2	193	6	164	4	0.078	0.006	10.6	0.75	16.49	1.17
GEMS_N720_6	1:48:58.649	-12:48:18.681	1770	7	220	21	165	14	0.033	0.005	3.7	0.59	5.76	0.92
GEMS_N720_7	1:49:35.781	-13:29:37.625	1450	8	252	24	165	16	0.032	0.005	3.7	0.54	5.76	0.84
GEMS_N720_8	1:44:59.449	-16:26:18.797	1585	7	152	21	117	14	0.029	0.006	2.2	0.57	3.42	0.89
GEMS_N1052_1	2:39:25.731	-8:09:40.445	1266	3	299	9	244	6	0.070	0.006	13.1	0.80	10.00	0.61
GEMS_N1052_2	2:41:01.566	-6:55:18.063	1297	1	194	3	183	2	0.174	0.010	21.8	1.10	16.64	0.84
GEMS_N1052_3	2:45:59.555	-7:34:03.815	1405	2	332	6	293	4	0.251	0.013	59.6	2.09	45.50	1.60
GEMS_N1052_4	2:49:12.555	-7:49:54.822	1329	1	190	3	172	2	0.192	0.011	29.2	1.38	22.29	1.05
GEMS_N1052_5	2:40:29.765	-6:05:59.947	1325	1	97	3	84	2	0.135	0.008	10.0	0.68	7.63	0.52
GEMS_N1052_6	2:41:42.039	-7:55:29.289	1373	4	136	12	81	8	0.047	0.005	3.8	0.45	2.90	0.35
GEMS_N1052_7	2:40:26.810	-8:25:17.977	1371	1	118	3	100	2	0.463	0.024	44.2	2.37	33.74	1.81
GEMS_N1052_8	2:35:26.590	-9:20:53.242	1504	1	278	3	256	2	0.183	0.010	32.6	1.40	24.89	1.07
GEMS_N1052_9	2:33:56.139	-6:22:24.736	1411	2	57	6	40	4	0.063	0.005	2.6	0.33	1.98	0.25
GEMS_N1052_10	2:49:13.865	-8:07:17.779	1419	4	155	12	80	8	0.080	0.007	7.6	0.68	5.80	0.52
GEMS_N1052_11	2:35:31.894	-7:08:58.737	1532	1	91	3	74	2	0.243	0.013	17.6	1.10	13.43	0.84
GEMS_N1052_12	2:30:28.038	-10:44:12.632	2100	2	139	6	114	4	0.082	0.006	7.3	0.60	5.57	0.46
GEMS_N1052_13	2:42:44.220	-7:22:56.063	1420	3	55	9	48	6	0.025	0.005	0.9	0.30	0.69	0.23
GEMS_N1052_14	2:43:35.611	-6:38:23.618	1408	1	56	3	41	2	0.129	0.008	5.0	0.49	3.82	0.38
GEMS_N1052_15	2:38:32.127	-6:38:55.517	1470	6	168	18	141	12	0.023	0.005	2.7	0.57	2.06	0.44
GEMS_N1332_1	3:16:22.347	-24:16:07.601	2087	3	113	9	76	6	0.159	0.015	9.7	1.19	9.98	1.22
GEMS_N1332_2 ¹	3:33:47.980	-19:29:33.799	1964	2	233	6	200	4	0.216	0.012	38.6	1.67	39.72	1.72
GEMS_N1332_3 ¹	3:33:40.004	-21:29:10.175	1860	2	212	6	196	4	0.100	0.007	13.0	0.84	13.38	0.86
GEMS_N1332_4	3:23:42.628	-19:44:14.250	1846	2	126	6	113	4	0.087	0.008	8.9	0.80	9.16	0.82
GEMS_N1332_5 ¹	3:35:36.163	-21:22:01.989	1808	3	170	9	132	6	0.057	0.005	6.1	0.52	6.28	0.54
GEMS_N1332_6	3:29:57.124	-22:19:45.366	1767	4	101	12	60	8	0.074	0.008	3.9	0.60	4.01	0.61
GEMS_N1332_7	3:24:29.555	-21:32:14.609	1588	1	346	3	330	2	0.142	0.009	26.6	1.31	27.37	1.35
GEMS_N1332_8	3:27:29.867	-21:17:03.795	1696	10	364	30	188	20	0.036	0.005	6.0	0.69	6.17	0.71
GEMS_N1332_9	3:19:40.437	-19:24:43.686	1577	1	285	3	268	2	0.225	0.013	36.9	1.65	37.97	1.70
GEMS_N1332_10	3:18:43.358	-23:48:08.206	1538	1	98	3	82	2	0.140	0.009	9.8	0.74	10.09	0.76
GEMS_N1332_11	3:24:00.101	-18:34:48.091	1453	9	293	27	181	18	0.044	0.007	4.6	0.73	4.73	0.75
GEMS_N1332_12	3:24:51.240	-21:19:05.317	1333	2	68	6	45	4	0.132	0.010	6.6	0.70	6.79	0.72
GEMS_N1332_13	3:37:49.595	-24:25:43.446	1512	4	209	12	157	8	0.163	0.016	20.9	1.86	21.51	1.92
GEMS_N1332_14	3:32:42.148	-24:07:42.582	1913	3	194	9	164	6	0.061	0.007	4.2	0.57	4.32	0.58
GEMS_N1332_15	3:35:28.893	-21:08:27.717	1514	9	138	27	80	18	0.028	0.006	1.6	0.48	1.65	0.49
GEMS_N1332_16	3:23:27.444	-19:17:31.585	1553	3	52	9	33	6	0.092	0.010	3.1	0.59	3.19	0.60

Table A2. HI detections of the galaxies in groups. The columns are the same as Table A1.

(1)	(2)	(3)	(4)	(5)	(6)	(7)	(8)	(9)	(10)	(11)	(12)	(13)	(14)	(15)
GEMS_N1407_1 ¹	3:33:45.965	-19:29:22.958	1969	2	227	6	199	4	0.224	0.013	37.4	1.69	38.49	1.74
GEMS_N1407_2	3:32:11.129	-17:41:02.037	1943	3	200	9	152	6	0.084	0.006	11.5	0.70	11.83	0.72
GEMS_N1407_3 ¹	3:33:39.753	-21:30:30.801	1869	2	229	6	212	4	0.089	0.008	15.4	1.06	15.85	1.10
GEMS_N1407_4 ¹	3:35:22.788	-21:18:38.901	1816	3	182	9	148	6	0.071	0.007	7.9	0.74	8.13	0.76
GEMS_N1407_5	3:42:36.925	-17:26:04.314	1712	5	223	15	152	10	0.058	0.007	6.9	0.78	7.10	0.80
GEMS_N1407_6	3:34:42.734	-19:04:25.312	1604	2	370	6	363	4	0.034	0.005	4.9	0.57	5.04	0.59
GEMS_N1407_7	3:29:32.760	-17:47:04.322	1530	1	146	3	130	2	0.134	0.008	14.6	0.85	15.03	0.87
GEMS_N1407_8	3:38:11.118	-18:54:57.297	1192	7	245	21	161	14	0.043	0.006	5.1	0.68	5.25	0.70
GEMS_N1566_1	4:12:10.61	-58:34:17.40	1466	3	102	9	55	6	0.106	0.009	6.1	0.73	6.34	0.76
GEMS_N1566_2	4:10:51.16	-56:30:31.51	1310	6	129	18	104	12	0.028	0.006	1.9	0.53	1.97	0.55
GEMS_N1566_3	4:12:38.84	-57:45:49.62	1176	2	214	6	189	4	0.076	0.006	8.7	0.63	9.04	0.66
GEMS_N1566_4	4:27:25.22	-57:27:21.05	1215	5	137	15	75	10	0.048	0.006	3.5	0.49	3.64	0.51
GEMS_N1566_5	4:09:41.61	-56:06:55.80	796	3	324	9	248	6	0.382	0.022	73.5	3.18	76.37	3.31
GEMS_N1566_6	4:22:41.62	-56:16:58.66	1350	3	76	9	52	6	0.049	0.005	2.5	0.40	2.60	0.42
GEMS_N1566_7	4:14:40.37	-56:04:25.17	1298	6	344	18	189	12	0.140	0.013	23.2	1.69	24.10	1.76
GEMS_N1566_8	4:17:56.28	-55:57:06.31	1370	2	218	6	193	4	0.124	0.008	17.0	0.91	17.66	0.95
GEMS_N1566_9	4:07:10.06	-55:18:01.11	1068	2	119	6	99	4	0.073	0.006	5.9	0.54	6.13	0.56
GEMS_N1566_10	4:19:53.33	-54:56:45.66	1502	1	223	3	200	2	1.040	0.053	149.4	6.50	155.23	6.75
GEMS_N1566_11	4:27:45.38	-55:01:07.73	1572	3	174	9	94	6	0.283	0.017	32.0	1.81	33.25	1.88
GEMS_N1566_12	4:03:56.23	-54:05:04.20	1180	2	381	6	357	4	0.101	0.007	15.9	0.86	16.52	0.90
GEMS_N1566_13	4:05:41.94	-52:41:00.59	902	2	104	6	88	4	0.079	0.008	4.9	0.66	5.09	0.69
GEMS_N1808_1	5:16:36.579	-37:05:56.048	1344	1	293	3	275	2	0.297	0.016	55.6	2.22	37.86	1.51
GEMS_N1808_2	5:19:18.508	-37:06:35.334	1340	2	91	6	76	4	0.090	0.007	5.0	0.51	3.40	0.35
GEMS_N1808_3	5:21:05.551	-36:56:41.001	1292	2	160	6	133	4	0.118	0.008	13.3	0.87	9.06	0.59
GEMS_N1808_4	5:05:13.040	-37:58:49.413	1206	2	324	6	298	4	0.152	0.009	37.8	1.46	25.74	0.99
GEMS_N1808_5	5:07:42.077	-37:30:23.888	1002	2	311	6	254	4	0.307	0.016	70.4	2.48	47.93	1.69
GEMS_N1808_6	5:10:01.901	-36:57:41.750	1041	2	189	6	164	4	0.156	0.009	21.4	1.06	14.57	0.72
GEMS_N1808_7	5:08:05.366	-38:18:19.704	1020	1	132	3	115	2	0.620	0.031	64.6	3.28	43.99	2.23
GEMS_N3557_1	11:10:52.547	-37:26:30.563	2450	2	321	6	280	4	0.119	0.007	27.6	1.09	117.45	4.63
GEMS_N3557_2	11:11:14.459	-36:57:19.026	2470	6	286	18	130	12	0.068	0.006	9.9	0.70	42.13	2.97
GEMS_N3557_3	11:17:01.328	-34:56:42.410	2607	1	247	3	226	2	0.136	0.008	23.7	1.08	100.86	4.61
GEMS_N3557_4	11:10:49.023	-35:59:25.033	2768	3	296	9	264	6	0.071	0.006	11.8	0.81	50.22	3.46
GEMS_N3557_5	11:03:47.797	-38:45:41.909	2690	2	146	6	126	4	0.048	0.005	3.8	0.43	16.17	1.82
GEMS_N3557_6	11:21:56.051	-37:52:27.196	2754	2	142	6	120	4	0.062	0.005	6.6	0.56	28.09	2.39
GEMS_N3557_7	11:12:14.333	-38:04:24.742	2730	3	149	9	128	6	0.033	0.004	2.7	0.40	11.49	1.71
GEMS_N3557_8	11:12:23.782	-36:28:02.396	2933	3	229	9	199	6	0.049	0.005	7.8	0.71	33.19	3.02
GEMS_N3557_9	10:59:40.443	-37:23:15.073	2922	6	144	18	112	12	0.025	0.004	2.3	0.44	9.79	1.88
GEMS_N3557_10	11:07:05.243	-37:10:29.839	3119	4	472	12	395	8	0.059	0.005	11.9	0.76	50.64	3.24
GEMS_N3557_11	11:18:07.861	-40:35:34.768	3106	3	307	9	253	6	0.115	0.009	20.3	1.19	86.39	5.09
GEMS_N3557_12	11:01:02.095	-38:00:12.367	3591	2	159	6	129	4	0.110	0.007	11.1	0.77	47.24	3.26
GEMS_N3557_13	11:11:11.135	-36:45:56.109	2443	3	293	9	273	6	0.055	0.008	7.360	0.89	31.320	3.800
GEMS_N3783_1	11:34:18.389	-37:09:39.085	3202	7	340	21	250	14	0.058	0.008	11.1	1.18	33.89	3.61
GEMS_N3783_2	11:31:32.407	-36:18:53.054	2733	11	142	33	36	22	0.041	0.008	1.9	0.57	5.80	1.74
GEMS_N3783_3	11:28:05.772	-36:32:44.950	3018	2	284	6	253	4	0.229	0.013	38.0	1.77	116.03	5.40
GEMS_N3783_4	11:49:39.599	-37:30:49.655	3055	2	53	6	36	4	0.201	0.014	7.4	0.89	22.59	2.71
GEMS_N3783_5	11:49:00.993	-37:29:47.332	2933	3	157	9	119	6	0.150	0.013	16.6	1.37	50.69	4.18
GEMS_N3783_6	11:49:33.388	-38:50:39.854	2989	3	178	9	155	6	0.095	0.009	12.5	1.08	38.17	3.29
GEMS_N3783_7	11:38:50.962	-37:47:37.741	2923	2	171	6	141	4	0.121	0.010	12.4	1.01	37.86	3.09
GEMS_N3783_8	11:37:54.347	-37:56:04.265	2947	6	215	18	158	12	0.064	0.009	6.9	0.95	21.07	2.90
GEMS_N3783_9	11:35:42.955	-38:02:07.807	2705	6	521	18	464	12	0.069	0.010	19.5	1.80	59.54	5.48
GEMS_N3783_10	11:26:06.212	-37:51:26.206	2810	5	99	15	53	10	0.056	0.008	2.5	0.56	7.63	1.70
GEMS_N3783_11	11:21:57.181	-37:46:44.550	2741	10	141	30	82	20	0.062	0.015	4.0	1.26	12.21	3.86
GEMS_N3783_12	11:29:42.717	-37:16:59.336	3049	7	235	21	212	14	0.026	0.007	3.7	0.80	11.30	2.45

¹ Note three sources from the NGC 1407 group were also detected in the NGC 1332 group: GEMS_N1407_1 = GEMS_N1332_2, GEMS_N1407_3 = GEMS_N1332_3, GEMS_N1407_4 = GEMS_N1332_5. These sources are listed in both groups so the reader can compare and contrast the derived values.

Table A3. H1 detections of the galaxies in groups. The columns are the same as Table A1.

(1)	(2)	(3)	(4)	(5)	(6)	(7)	(8)	(9)	(10)	(11)	(12)	(13)	(14)	(15)
GEMS_N3923_1	11:53:21.485	-28:33:23.599	1706	1	287	3	272	2	0.313	0.017	63.7	2.45	68.09	2.62
GEMS_N3923_2	11:53:59.368	-27:21:12.797	1634	2	132	6	113	4	0.081	0.007	6.7	0.62	7.16	0.66
GEMS_N3923_3	11:45:40.039	-28:21:51.750	1842	1	196	3	175	2	0.160	0.009	23.1	1.16	24.69	1.25
GEMS_N3923_4	11:48:35.358	-27:22:15.794	1875	3	192	9	110	6	0.109	0.007	12.6	0.77	13.47	0.83
GEMS_N3923_5	11:53:41.920	-26:59:10.496	1908	5	148	15	105	10	0.050	0.007	5.0	0.70	5.34	0.75
GEMS_N3923_6	11:52:35.295	-26:55:26.144	2027	5	373	15	303	10	0.143	0.016	32.4	2.40	34.63	2.57
GEMS_N3923_7	11:59:16.997	-28:55:30.793	2022	1	192	3	176	2	0.186	0.011	20.6	1.21	22.02	1.30
GEMS_N3923_8	11:43:44.599	-30:38:36.454	1987	2	149	6	135	4	0.069	0.006	6.7	0.60	7.16	0.64
GEMS_N3923_9	12:01:59.521	-30:14:36.611	2059	4	98	12	75	8	0.042	0.007	2.1	0.52	2.24	0.55
GEMS_N3923_10	12:03:08.055	-29:06:10.678	2202	3	121	9	89	6	0.139	0.012	10.7	1.05	11.44	1.13
GEMS_N3923_11	11:50:17.353	-30:04:33.781	1600	3	70	9	61	6	0.026	0.005	1.3	0.36	1.39	0.39
GEMS_N3923_12	11:48:44.460	-28:17:24.017	1938	1	118	3	104	2	0.252	0.013	25.5	1.37	27.26	1.47
GEMS_N3923_13	11:57:22.427	-28:06:15.341	2131	1	37	3	28	2	0.067	0.006	1.7	0.29	1.82	0.31
GEMS_N4636_1	12:47:48.791	4:20:46.733	986	1	65	3	44	2	0.637	0.032	29.0	2.22	12.64	0.97
GEMS_N4636_2	12:32:46.834	0:06:04.089	1127	1	317	3	301	2	0.402	0.021	87.5	3.11	38.13	1.36
GEMS_N4636_3	12:49:46.875	2:51:58.984	1158	1	223	3	214	2	0.053	0.004	7.5	0.55	3.27	0.24
GEMS_N4636_4	12:44:29.212	0:29:24.114	1180	1	120	3	107	2	0.139	0.008	12.7	0.79	5.53	0.34
GEMS_N4636_5	12:33:51.088	3:36:41.541	1134	2	41	6	29	4	0.052	0.005	1.5	0.26	0.65	0.11
GEMS_N4636_6	12:39:49.367	1:39:51.479	1222	4	169	12	101	8	0.049	0.005	4.8	0.47	2.09	0.20
GEMS_N4636_7	12:53:31.313	2:04:43.774	1217	4	110	12	38	8	0.064	0.006	3.4	0.43	1.48	0.19
GEMS_N4636_8	12:33:02.136	4:35:35.262	1223	4	101	12	62	8	0.038	0.004	2.1	0.34	0.92	0.15
GEMS_N4636_9	12:36:40.018	3:07:30.296	1441	1	128	3	117	2	0.067	0.005	6.6	0.48	2.88	0.21
GEMS_N4636_10	12:32:28.618	0:24:20.325	1529	1	167	3	154	2	0.297	0.015	34.2	1.70	14.90	0.74
GEMS_N4636_11	12:34:08.975	2:38:59.839	1737	1	376	3	356	2	0.413	0.021	96.2	3.29	41.92	1.43
GEMS_N4636_12	12:42:34.107	-0:04:51.599	1722	1	246	3	223	2	0.239	0.013	46.3	1.84	20.18	0.80
GEMS_N4636_13	12:41:13.093	1:25:08.767	1701	3	168	9	104	6	0.079	0.006	8.6	0.63	3.75	0.27
GEMS_N4636_14	12:34:27.211	2:13:13.437	1806	1	342	3	324	2	0.329	0.017	73.3	2.61	31.94	1.14
GEMS_N4636_15	12:31:38.089	3:56:40.982	1733	1	175	3	154	2	0.334	0.017	43.5	2.03	18.96	0.89
GEMS_N4636_16	12:32:43.880	2:41:14.371	1731	2	164	6	147	4	0.099	0.007	12.1	0.75	5.27	0.33
GEMS_N4636_17	12:31:17.108	0:59:13.442	2296	4	67	12	30	8	0.052	0.007	1.7	0.38	0.74	0.17
GEMS_N4636_18	12:34:13.033	1:45:40.391	2472	4	105	12	94	8	0.024	0.005	1.4	0.37	0.61	0.16
GEMS_N4636_19	12:37:32.697	4:44:20.324	1632	7	60	21	27	14	0.022	0.005	0.7	0.27	0.31	0.12
GEMS_N4636_20	12:39:22.679	-0:36:01.896	1069	1	214	3	198	2	1.131	0.060	172.0	7.62	74.95	3.32
GEMS_N4636_21	12:45:18.952	-0:29:00.355	1518	2	397	6	324	4	0.380	0.020	84.7	3.09	36.91	1.35
GEMS_N4636_22	12:55:05.564	0:07:09.054	1320	1	186	3	175	2	0.182	0.014	21.2	1.51	9.24	0.66
GEMS_N5044_1	13:14:09.927	-16:41:41.635	3075	5	204	15	148	10	0.039	0.005	4.4	0.53	8.72	1.06
GEMS_N5044_2	13:12:36.812	-15:51:07.902	2928	6	183	18	32	12	0.087	0.007	6.6	0.66	13.08	1.30
GEMS_N5044_3	13:18:29.023	-14:36:24.290	2897	3	236	9	196	6	0.086	0.007	11.2	0.87	22.19	1.72
GEMS_N5044_4	13:03:09.633	-17:23:16.021	2967	1	56	3	33	2	0.208	0.012	8.1	0.76	16.05	1.51
GEMS_N5044_5	13:05:37.270	-15:46:58.451	2911	3	118	9	93	6	0.049	0.005	3.9	0.49	7.73	0.98
GEMS_N5044_6	13:19:19.577	-14:49:02.816	2749	2	401	6	380	4	0.069	0.006	16.5	0.88	32.69	1.74
GEMS_N5044_7	13:10:59.343	-15:20:44.288	2828	8	386	24	315	16	0.026	0.005	4.3	0.63	8.52	1.25
GEMS_N5044_8	13:12:38.338	-17:32:18.269	2753	4	396	12	346	8	0.051	0.005	11.2	0.75	22.19	1.48
GEMS_N5044_9	13:15:08.786	-17:59:08.810	2773	2	63	6	40	4	0.090	0.007	3.9	0.49	7.73	0.96
GEMS_N5044_10	13:20:14.216	-14:25:41.013	2748	2	64	6	42	4	0.108	0.008	4.9	0.56	9.71	1.11
GEMS_N5044_11	13:19:58.070	-17:17:43.872	2685	3	122	9	97	6	0.063	0.006	4.4	0.51	8.72	1.01
GEMS_N5044_12	13:16:58.645	-16:17:44.175	2624	3	310	9	277	6	0.047	0.005	9.2	0.70	18.23	1.40
GEMS_N5044_13	13:13:21.838	-16:05:40.043	2694	4	152	12	26	8	0.133	0.009	10.3	0.79	20.41	1.57
GEMS_N5044_14	13:08:05.016	-14:44:53.255	2599	1	112	3	101	2	0.072	0.006	5.6	0.54	11.10	1.06
GEMS_N5044_15	13:03:18.888	-14:45:52.821	2572	4	137	12	73	8	0.075	0.006	5.2	0.56	10.30	1.10
GEMS_N5044_16	13:13:36.158	-15:25:54.235	2502	1	91	3	73	2	0.207	0.012	15.4	1.05	30.51	2.07
GEMS_N5044_17	13:18:58.428	-17:37:14.239	2494	3	108	9	68	6	0.067	0.006	4.7	0.52	9.31	1.03
GEMS_N5044_18	13:11:36.133	-14:40:40.125	2488	4	141	12	100	8	0.040	0.005	3.2	0.46	6.34	0.91
GEMS_N5044_19	13:17:18.638	-17:17:59.994	2520	2	230	6	219	4	0.053	0.006	7.3	0.67	14.46	1.33
GEMS_N5044_20	13:16:57.879	-16:36:21.407	1836	2	141	6	107	4	0.085	0.006	6.8	0.58	13.47	1.15
GEMS_N5044_21	13:24:52.255	-19:41:24.120	1947	5	243	15	172	10	0.244	0.025	29.3	2.85	58.05	5.65
GEMS_N5044_22	13:05:20.342	-16:55:08.371	2834	3	182	9	156	6	0.056	0.006	4.1	0.50	8.12	1.00
GEMS_N5044_23	13:09:33.913	-16:36:24.423	2576	2	354	6	333	4	0.114	0.007	28.8	1.12	57.06	2.22

Table A4. H1 detections of the galaxies in groups. The columns are the same as Table A1.

(1)	(2)	(3)	(4)	(5)	(6)	(7)	(8)	(9)	(10)	(11)	(12)	(13)	(14)	(15)
GEMS_N7144_1	21:45:08.395	-49:00:43.150	1598	2	114	6	71	4	0.315	0.017	21.40	1.46	26.21	1.79
GEMS_N7144_2	22:09:20.739	-47:11:18.717	1722	7	460	21	210	14	0.109	0.009	21.89	1.29	26.81	1.58
GEMS_N7144_3	21:45:49.101	-48:49:13.536	1617	3	150	9	116	6	0.096	0.008	8.73	0.83	10.69	1.02
GEMS_N7144_4	21:55:07.416	-50:38:42.157	1871	3	218	9	196	6	0.077	0.008	10.25	0.95	12.55	1.16
GEMS_N7144_5	21:55:38.108	-49:15:06.927	1860	2	97	6	83	4	0.066	0.008	4.83	0.68	5.92	0.83
GEMS_N7144_6	21:42:42.971	-47:55:24.345	1956	3	248	9	196	6	0.141	0.010	20.26	1.22	24.81	1.50
GEMS_N7144_7	21:41:02.448	-46:40:18.955	1958	4	78	12	27	8	0.073	0.008	2.44	0.47	2.99	0.57
GEMS_N7144_8	21:42:44.625	-51:15:25.309	2075	3	152	9	129	6	0.076	0.008	7.00	0.79	8.57	0.96
GEMS_N7714_1	23:41:33.273	3:45:17.985	2891	4	261	12	152	8	0.169	0.011	25.75	1.39	92.27	4.99
GEMS_N7714_2	23:36:25.686	2:08:44.429	2721	5	325	15	205	10	0.112	0.009	19.53	1.22	69.99	4.36
GEMS_N7714_3	23:37:31.755	0:23:59.861	2674	3	164	9	141	6	0.084	0.008	9.32	0.88	33.40	3.17
GEMS_N7714_4	23:46:44.349	3:42:03.825	2901	3	300	9	235	6	0.162	0.011	25.56	1.38	91.59	4.95
GEMS_N7714_5	23:36:33.185	0:20:41.739	2588	3	286	9	238	6	0.123	0.009	23.57	1.32	84.46	4.75
GEMS_N7714_6	23:35:22.987	1:10:59.750	2599	2	103	6	84	4	0.082	0.008	5.63	0.69	20.17	2.48
GEMS_N7714_7	23:45:18.649	3:41:28.458	2755	7	489	21	212	14	0.131	0.010	24.01	1.33	86.04	4.78
GEMS_HCG90_1	22:01:19.670	-32:36:12.937	2271	2	181	6	165	4	0.081	0.008	8.10	0.83	24.73	2.54
GEMS_HCG90_2	22:01:28.086	-31:33:10.938	2353	6	370	18	282	12	0.060	0.008	12.05	1.11	36.79	3.39
GEMS_HCG90_3	22:03:49.062	-32:18:59.783	2550	3	288	9	266	6	0.070	0.008	13.34	1.11	40.73	3.39
GEMS_HCG90_4	22:07:02.414	-31:03:03.066	2583	5	294	15	200	10	0.084	0.008	11.82	0.99	36.09	3.04
GEMS_HCG90_5	21:55:35.591	-34:44:08.965	2614	2	169	6	133	4	0.156	0.010	17.96	1.16	54.84	3.53
GEMS_HCG90_6	21:56:48.419	-34:34:30.401	2656	6	374	18	230	12	0.087	0.008	15.52	1.13	47.39	3.45
GEMS_HCG90_7	22:01:27.658	-35:14:35.759	2515	2	200	6	185	4	0.088	0.008	6.97	0.76	21.28	2.31
GEMS_HCG90_8	22:08:37.651	-34:17:58.435	2670	5	207	15	80	10	0.115	0.009	11.12	0.91	33.95	2.79
GEMS_HCG90_9	22:03:08.521	-33:53:03.327	2720	6	453	18	367	12	0.060	0.008	11.94	1.10	36.46	3.37
GEMS_HCG90_10	22:08:43.330	-30:56:29.547	2560	3	58	9	46	6	0.044	0.007	1.57	0.45	4.79	1.37
GEMS_HCG90_11	22:06:19.336	-31:04:41.189	2596	4	183	12	44	8	0.144	0.010	7.54	0.75	23.02	2.28
GEMS_HCG90_12	22:01:48.903	-31:54:43.334	2316	12	104	36	34	24	0.028	0.007	2.97	0.76	9.07	2.31
GEMS_IC1459_1	23:02:12.289	-39:34:04.659	1198	1	249	3	234	2	0.31	0.02	52.06	2.26	90.74	3.94
GEMS_IC1459_2	22:59:30.939	-37:41:37.029	1299	2	226	6	196	4	0.14	0.01	21.83	1.27	38.05	2.22
GEMS_IC1459_3	23:00:18.564	-37:11:21.982	1239	3	74	9	42	6	0.087	0.008	3.62	0.55	6.31	0.95
GEMS_IC1459_4	22:55:43.115	-34:34:17.800	1282	8	195	24	83	16	0.052	0.007	4.04	0.68	7.04	1.18
GEMS_IC1459_5	23:02:15.438	-37:04:55.632	1372	2	137	6	121	4	0.104	0.009	11.04	0.92	19.24	1.61
GEMS_IC1459_6	22:56:28.173	-37:01:55.086	1446	2	233	6	207	4	0.180	0.011	28.00	1.46	48.81	2.55
GEMS_IC1459_7	22:56:42.596	-36:14:16.044	1667	2	242	6	228	4	0.123	0.009	17.25	1.13	30.07	1.98
GEMS_IC1459_8	22:56:47.404	-37:19:42.368	1789	3	141	9	129	6	0.052	0.007	4.30	0.70	7.50	1.22
GEMS_IC1459_9	22:57:21.286	-36:35:09.619	1790	6	192	18	96	12	0.072	0.008	5.59	0.71	9.74	1.24
GEMS_IC1459_10	23:00:49.061	-35:22:07.512	1773	4	214	12	172	8	0.062	0.008	8.41	0.92	14.66	1.60
GEMS_IC1459_11	22:58:05.708	-35:48:43.725	1950	3	199	9	101	6	0.390	0.021	38.19	2.11	66.57	3.67
GEMS_IC1459_12	22:56:41.430	-36:44:14.421	2101	2	216	6	180	4	0.164	0.011	23.49	1.33	40.94	2.31
GEMS_IC1459_13	22:45:42.249	-39:21:09.628	2279	5	233	15	137	10	0.087	0.008	8.87	0.85	15.46	1.49
GEMS_IC1459_14	22:43:37.768	-39:54:04.091	2147	2	169	6	145	4	0.219	0.013	24.26	1.41	42.29	2.45
GEMS_IC1459_15	22:58:03.586	-33:45:54.083	1718	6	382	18	346	12	0.043	0.007	9.00	1.09	15.69	1.90
GEMS_IC1459_16	23:09:02.363	-39:48:58.259	1787	4	96	12	80	8	0.037	0.007	2.32	0.59	4.04	1.03
GEMS_IC1459_17	22:53:19.129	-38:47:56.731	879	5	72	15	40	10	0.041	0.007	1.52	0.46	2.65	0.79
GEMS_IC1459_18	23:01:38.433	-36:30:33.653	1668	12	149	36	83	24	0.027	0.007	1.63	0.57	2.84	0.99

Table B1. Optical counterparts to the H I detections. The columns are as follows: (1) GEMS H I catalogue designation; (2) Systemic velocity, V_{sys} , derived from the H I spectrum, in km s^{-1} ; (3) distance of H I source position from optically catalogued galaxy position, in arcmin; (4) name of optically catalogued galaxy; (5) 6dFGS name; (6) & (7) Position of optically catalogued source, α, δ (J2000) [h m s][$^{\circ}$ $''$]; (8) Systemic velocity of optically catalogued source in km s^{-1} .

(1)	(2)	(3)	(4)	(5)	(6)	(7)	(8)
GEMS_N524_1	2898	0.71	UGC 00993 NED01	...	01:25:34.20	07:59:24.0	2926
GEMS_N524_1	2898	0.76	UGC 00993 NED02	...	01:25:35.12	07:59:27.0	2928
GEMS_N524_2	2778	3.45	UGC 00989	...	01:25:29.60	07:33:41.0	2788
GEMS_N524_3	2740	7.95	VV 730	...	01:23:19.50	07:47:42.0	2700
GEMS_N524_3	2740	0.82	UGC 00964	...	01:24:35.06	07:43:16.2	2737
GEMS_N524_4	2728	1.91	UGC 00941	...	01:23:32.42	06:57:38.0	2728
GEMS_N524_5	2549	3.32	UGC 00990	...	01:25:24.00	10:47:49.0	2536
GEMS_N524_6	2348	0.56	UGC 00803	...	01:15:22.91	08:05:57.5	2342
GEMS_N524_7	2335	2.24	UGC 00942	...	01:23:43.70	06:41:29.0	2335
GEMS_N524_8	2687	4.87	VV 730	...	01:23:19.50	07:47:42.0	2700
GEMS_N524_9	2430	0.84	LEDA 093841	...	01:27:37.30	08:50:24.0	2435
<hr/>							
GEMS_N720_1	1635	1.04	MCG -03-05-014	...	01:41:35.92	-16:08:49.6	1637
GEMS_N720_2	1154	0.00	MCG -03-05-017	...	01:42:58.50	-16:07:45.0	1154
GEMS_N720_3	1742	0.68	KUG 0144-147	J0146553-142710	01:46:55.27	-14:27:09.5	1711
GEMS_N720_4	1613	0.79	ARP 004	...	01:48:25.67	-12:22:55.3	1614
GEMS_N720_5	1865	0.38	UGCA 022	...	01:56:59.14	-11:46:47.8	1853
GEMS_N720_6	1770
GEMS_N720_7	1450	4.66	KUG 0147-138	...	01:49:37.92	-13:34:15.4	1449
GEMS_N720_8	1585	1.08	APMUKS(BJ) B014238.60-164056.8	J0145037-162556	01:45:03.67	-16:25:55.7	1588
<hr/>							
GEMS_N1052_1	1266	1.89	NGC 1035	...	02:39:29.09	-08:07:58.6	1241
GEMS_N1052_1	1266	1.68	6dF J0239299-080821	J0239299-080821	02:39:29.92	-08:08:21.1	1393
GEMS_N1052_2	1297	0.88	NGC 0961	...	02:41:02.46	-06:56:09.1	1295
GEMS_N1052_3	1405	0.66	NGC 1084	...	02:45:59.93	-07:34:43.1	1407
GEMS_N1052_4 ¹	1329	0.81	NGC 1110	...	02:49:09.57	-07:50:15.2	1333
GEMS_N1052_5	1325	0.40	UGCA 038	...	02:40:30.19	-06:06:23.0	1327
GEMS_N1052_6	1351	1.96	SDSS J024149.95-075530.1	...	02:41:49.96	-07:55:30.0	1372
GEMS_N1052_7	1371	1.00	NGC 1042	J0240240-082601	02:40:23.97	-08:26:01.0	1411
GEMS_N1052_8	1504	0.55	NGC 0988	J0235277-092122	02:35:27.73	-09:21:21.6	1551
GEMS_N1052_9	1411	0.84	[RC3] 0231.5-0635	...	02:33:57.04	-06:21:36.2	1410
GEMS_N1052_10 ¹	1418	0.42	[MMB2004] J0249-0806	...	02:49:13.42	-08:06:53.2	...
GEMS_N1052_11	1532	0.77	USGC S092 NED09	...	02:35:28.79	-07:08:59.0	1532
GEMS_N1052_11	1532	0.63	6dF J0235320-070936	J0235320-070936	02:35:32.00	-07:09:36.3	1554
GEMS_N1052_11	1532	0.35	NGC 0991	...	02:35:32.69	-07:09:16.0	1532
GEMS_N1052_12	2100	0.96	DDO 023	...	02:30:25.46	-10:44:55.6	2110
GEMS_N1052_13**	1420	9.59	SDSS J024246.84-073230.3	...	02:42:46.84	-07:32:30.4	1344
GEMS_N1052_14	1408	1.91	MCG -01-08-001	...	02:43:42.80	-06:39:05.0	1410
GEMS_N1052_15	1466	1.73	NGC 1022	...	02:38:32.70	-06:40:38.7	1453

Table B2. Optical counterparts to the H I detections. The columns are the same as in Table B1.

(1)	(2)	(3)	(4)	(5)	(6)	(7)	(8)
GEMS_N1332_1	2087	5.01	UGCA 063	...	03:16:09.66	-24:12:02.2	2087
GEMS_N1332_2	1964	0.08	NGC 1359	...	03:33:47.71	-19:29:31.4	1973
GEMS_N1332_2	1964	6.61	ESO 548- G 043	...	03:34:10.53	-19:33:30.1	1931
GEMS_N1332_3 ⁴	1860	0.63	IC 1953	...	03:33:41.87	-21:28:43.1	1867
GEMS_N1332_4	1846	1.43	UGCA 068	...	03:23:47.25	-19:45:10.2	1838
GEMS_N1332_5	1808	4.40	IC 1962	...	03:35:37.49	-21:17:38.6	1806
GEMS_N1332_6	1767	4.48	NGC 1347	...	03:29:41.50	-22:17:06.0	1759
GEMS_N1332_7	1588	1.01	NGC 1325	J0324256-213238	03:24:25.57	-21:32:38.3	1588
GEMS_N1332_8	1696	3.63	2MASX J03273556-2113417	J0327356-211341	03:27:35.57	-21:13:41.4	1743
GEMS_N1332_9	1577	1.44	2MASXi J0319359-192344	J0319360-192345	03:19:35.99	-19:23:44.8	1696
GEMS_N1332_9	1577	0.16	NGC 1300	...	03:19:41.08	-19:24:40.9	1577
GEMS_N1332_10	1538	1.19	UGCA 065	...	03:18:43.14	-23:46:57.1	1538
GEMS_N1332_11**	1453	8.40	ESO 548- G 004	...	03:23:32.22	-18:39:59.7	1528
GEMS_N1332_12	1333	1.25	NGC 1325A	...	03:24:48.50	-21:20:10.0	1333
GEMS_N1332_13 ⁴	1513	6.51	NGC 1385	J0337283-243005	03:37:28.32	-24:30:04.7	1511
GEMS_N1332_14	1913	4.59	ESO 482- G 005	...	03:33:02.25	-24:07:58.3	1915
GEMS_N1332_15	1514	4.56	ESO 548- G 049	...	03:35:28.07	-21:13:01.3	1510
GEMS_N1332_16	1553	0.76	SGC 0321.2-1929	...	03:23:25.10	-19:17:00.0	1545
<hr/>							
GEMS_N1407_1	1969	0.43	NGC 1359	...	03:33:47.71	-19:29:31.4	1973
GEMS_N1407_1	1969	7.11	ESO 548- G 043	...	03:34:10.53	-19:33:30.1	1931
GEMS_N1407_2	1943	2.80	UGCA 077	...	03:32:19.17	-17:43:04.6	1961
GEMS_N1407_3 ⁴	1869	1.86	IC 1953	...	03:33:41.87	-21:28:43.1	1867
GEMS_N1407_4	1816	3.57	IC 1962	...	03:35:37.49	-21:17:38.6	1806
GEMS_N1407_5	1712	4.62	ESO 548- G 082	...	03:42:43.27	-17:30:26.0	1716
GEMS_N1407_6	1551	2.69	ESO 548- G 047	...	03:34:43.48	-19:01:44.1	1606
GEMS_N1407_7	1530	0.45	NGC 1345	J0329317-174642	03:29:31.69	-17:46:42.2	1556
GEMS_N1407_8	1192	7.13	NGC 1390	...	03:37:52.17	-19:00:30.1	1207
<hr/>							
GEMS_N1566_1	1466	1.20	IC2049	...	04:12:04.30	-58:33:25.0	1469
GEMS_N1566_2	1310	2.08	NGC 1536	J0410599-562850	04:10:59.86	-56:28:49.6	1274
GEMS_N1566_3	1176	1.66	NGC 1543	J0412432-574416	04:12:43.20	-57:44:16.4	1149
GEMS_N1566_4 ²	1215	0.00	LSBG157-081	...	04:27:25.22	-57:27:21.0	...
GEMS_N1566_5	796	1.44	NGC 1533	J0409518-560706	04:09:51.84	-56:07:06.4	764
GEMS_N1566_6 ²	1350	0.00	APMBGC157+016+068	...	04:22:41.62	-56:16:58.7	...
GEMS_N1566_7	1298	0.94	NGC 1546	J0414364-560340	04:14:36.38	-56:03:39.5	1238
GEMS_N1566_8	1370	1.16	IC 2058	...	04:17:54.35	-55:55:58.4	1379
GEMS_N1566_9	1068	1.73	IC 2032	...	04:07:03.04	-55:19:25.8	859
GEMS_N1566_10	1502	1.13	NGC 1566	...	04:20:00.42	-54:56:16.1	1504
GEMS_N1566_11	1572	1.17	NGC 1596	...	04:27:38.11	-55:01:40.1	1510
GEMS_N1566_11	1572	0.84	AM 0426-550	...	04:27:44.00	-55:01:57.0	1572
GEMS_N1566_11	1572	2.71	NGC 1602	...	04:27:54.97	-55:03:27.8	1568
GEMS_N1566_12	1180	1.33	NGC 1515	...	04:04:02.72	-54:06:00.2	1094
GEMS_N1566_13	902	4.04	NGC 1522	...	04:06:07.92	-52:40:06.3	905
<hr/>							
GEMS_N1808_1 ⁴	1344	0.49	ESO 362- G 011	...	05:16:38.80	-37:06:09.1	1367
GEMS_N1808_2	1339	0.30	ESO 362- G 016	...	05:19:18.48	-37:06:17.4	1344
GEMS_N1808_3	1292	0.78	ESO 362- G 019	...	05:21:04.18	-36:57:24.7	1299
GEMS_N1808_4	1206	0.27	NGC 1792	J0505144-375851	05:05:14.41	-37:58:50.5	1175
GEMS_N1808_5	1002	0.37	NGC 1808:[AB70] C	J0507423-373046	05:07:42.34	-37:30:46.1	969
GEMS_N1808_6	1041	0.46	NGC 1827	J0510046-365737	05:10:04.11	-36:57:34.9	1037
GEMS_N1808_7	1020	0.50	ESO 305- G 009	...	05:08:07.62	-38:18:33.5	1021

Table B3. Optical counterparts to the H I detections. The columns are the same as in Table B1.

(1)	(2)	(3)	(4)	(5)	(6)	(7)	(8)
GEMS_N3557_1	2453	7.89	NGC 3557:[ZM2000] 0017	...	11:10:13.60	-37:24:55.0	2447
GEMS_N3557_1	2453	0.87	NGC 3568	J1110486-372652	11:10:48.57	-37:26:52.3	2440
GEMS_N3557_2	2470	4.86	NGC 3573	J1111186-365232	11:11:18.57	-36:52:31.9	2410
GEMS_N3557_3	2607	0.89	ESO 377- G 034	J1117046-345719	11:17:04.50	-34:57:19.0	2586
GEMS_N3557_4	2768	1.57	ESO 377- G 021	J1110565-355900	11:10:56.54	-35:59:00.9	2750
GEMS_N3557_5	2690	0.00	ESO 318- G 033	...	11:03:47.80	-38:45:41.9	...
GEMS_N3557_6	2754	1.55	ESO 319- G 015	...	11:21:57.93	-37:53:57.8	2737
GEMS_N3557_7	2730	0.00	ESO 319- G 007	...	11:12:14.33	-38:04:24.7	...
GEMS_N3557_8	2933	3.13	ESO 377- G 024	J1112340-362541	11:12:33.99	-36:25:40.6	2836
GEMS_N3557_9	2921	0.00	NVSS J105929-372102	...	10:59:40.44	-37:23:15.1	...
GEMS_N3557_10	3119	0.48	NGC 3533	J1107076-371022	11:07:07.55	-37:10:21.5	3165
GEMS_N3557_11	3106	2.75	ESO 319- G 011	J1117534-403537	11:17:53.38	-40:35:37.1	3115
GEMS_N3557_12	3591	0.29	ESO 318- G 030	J1101022-375955	11:01:02.19	-37:59:54.9	3636
GEMS_N3557_13	2443	6.76	NGC 3573	J1111186-365232	11:11:18.57	-36:52:31.9	2410
GEMS_N3783_1 ³	3202	6.01	ESO 378- G 011	J1134436-371257	11:34:43.57	-37:12:57.4	3245
GEMS_N3783_2 ³	2733
GEMS_N3783_3 ³	3018	0.40	ESO 378- G 003	...	11:28:04.01	-36:32:33.8	3022
GEMS_N3783_4	3055	7.15	NGC 3903	J1149035-373102	11:49:03.54	-37:31:01.6	2983
GEMS_N3783_4	3055	1.74	AM 1147-371	...	11:49:41.70	-37:32:31.0	2964
GEMS_N3783_5	2933	2.03	ESO 378- G 023	J1148518-373042	11:48:51.83	-37:30:42.0	2932
GEMS_N3783_5	2933	1.34	NGC 3903	J1149035-373102	11:49:03.54	-37:31:01.6	2983
GEMS_N3783_6	2991	1.81	ESO 320- G 024	J1149261-384933	11:49:26.03	-38:49:33.4	3037
GEMS_N3783_6	2991	4.88	ESO 320- G 026	J1149503-384704	11:49:50.30	-38:47:03.9	2717
GEMS_N3783_6	2991	5.42	6dF J1149529-385431	J1149529-385431	11:49:52.93	-38:54:31.1	2707
GEMS_N3783_7	2923	3.94	NGC 3783	J1139017-374419	11:39:01.72	-37:44:18.9	2817
GEMS_N3783_8 ³	2947
GEMS_N3783_9	2705	5.17	NGC 3742	J1135325-375723	11:35:32.51	-37:57:23.0	2715
GEMS_N3783_9	2705	0.96	AM 1133-374	...	11:35:45.70	-38:01:20.0	2870
GEMS_N3783_9	2705	3.05	NGC 3749	J1135532-375951	11:35:53.21	-37:59:50.5	2742
GEMS_N3783_10	2810	0.04	ESO 319- G 020	...	11:26:06.00	-37:51:26.0	...
GEMS_N3783_11	2740	7.22	ESO 319- G 015	...	11:21:57.93	-37:53:57.8	2737
GEMS_N3783_12	3034	4.30	ESO 378- G 007	J1129480-371249	11:29:48.01	-37:12:49.2	3041
GEMS_N3923_1	1706	0.60	UGCA 250	J1153241-283311	11:53:24.06	-28:33:11.4	1699
GEMS_N3923_1	1706	1.30	2MASX J11532725-2833064	J1153273-283306	11:53:27.25	-28:33:06.0	1664
GEMS_N3923_2	1634	1.95	ESO 504- G 025	...	11:53:50.64	-27:21:00.0	1637
GEMS_N3923_3	1842	0.43	ESO 440- G 004	...	11:45:41.88	-28:21:59.5	1842
GEMS_N3923_4	1875	2.48	ESO 504- G 017	J1148464-272245	11:48:46.31	-27:22:45.0	1874
GEMS_N3923_5	1907	1.07	ESO 504- G 024	...	11:53:37.89	-26:59:44.9	1894
GEMS_N3923_6	2027	3.45	NGC 3936	J1152206-265421	11:52:20.59	-26:54:21.2	2011
GEMS_N3923_7	2022	1.22	ESO 440- G 037	J1159171-285418	11:59:17.09	-28:54:17.6	2009
GEMS_N3923_8 ⁴	1986	1.41	ESO 439- G 025	J1143458-303713	11:43:45.76	-30:37:13.4	1984
GEMS_N3923_9	2059	0.54	ESO 440- G 039	...	12:01:57.87	-30:14:12.5	2045
GEMS_N3923_10	2202	4.77	ESO 440- G 044	...	12:02:46.40	-29:05:33.0	2198
GEMS_N3923_11 ⁴	1600
GEMS_N3923_12	1938	0.31	UGCA 247	J1148456-281734	11:48:45.62	-28:17:34.9	1978
GEMS_N3923_13 ⁴	2131	2.20	[KK2000] 47	...	11:57:30.77	-28:07:27.2	2125*

Table B4. Optical counterparts to the H I detections. The columns are the same as in Table B1.

(1)	(2)	(3)	(4)	(5)	(6)	(7)	(8)
GEMS_N4636_1	986	0.85	NGC 4688	...	12:47:46.46	04:20:09.9	986
GEMS_N4636_1	986	0.91	SDSS J124747.00+041959.3	...	12:47:47.00	04:19:59.3	968
GEMS_N4636_1	986	5.92	CGCG 043-029 NED01	...	12:47:59.70	04:26:02.0	1041
GEMS_N4636_2	1127	6.92	UZC-CG 173	...	12:32:42.00	00:12:53.0	1394
GEMS_N4636_2	1127	0.89	NGC 4517	...	12:32:45.59	00:06:54.1	1131
GEMS_N4636_3	1158	1.16	UGC 07982	...	12:49:50.19	02:51:10.4	1155
GEMS_N4636_4	1180	1.32	UGC 07911	...	12:44:28.77	00:28:05.0	1183
GEMS_N4636_4	1180	5.59	VLA J124445.6-002536	...	12:44:45.60	00:25:36.0	1375
GEMS_N4636_5	1134	4.09	UGC 07715	...	12:33:55.69	03:32:46.2	1138
GEMS_N4636_6	1222	0.55	UGC 07824	...	12:39:50.31	01:40:21.5	1227
GEMS_N4636_7	1217	5.71	SDSS J125328.31+021023.4	...	12:53:28.31	02:10:23.5	977
GEMS_N4636_7	1217	5.40	NGC 4772	...	12:53:29.16	02:10:06.2	1040
GEMS_N4636_8	1232	1.56	VCC 1468	...	12:32:56.86	04:34:44.5	1233
GEMS_N4636_8	1232	1.18	SDSS J123258.82+043445.0	...	12:32:58.82	04:34:45.0	1207
GEMS_N4636_9	1441	1.13	UGC 07780	...	12:36:42.08	03:06:30.2	1441
GEMS_N4636_10	1529	0.97	NGC 4517A	...	12:32:28.15	00:23:22.8	1509
GEMS_N4636_11	1737	0.26	NGC 4527	...	12:34:08.50	02:39:13.7	1736
GEMS_N4636_12	1722	2.53	SDSS J124227.74+000253.5	...	12:42:27.75	00:02:53.6	1517
GEMS_N4636_12	1722	0.34	NGC 4632	...	12:42:32.80	00:04:47.0	1723
GEMS_N4636_13	1701	0.65	UGC 07841	...	12:41:11.60	01:24:37.0	1737
GEMS_N4636_14	1806	6.43	NGC 4533	...	12:34:22.02	02:19:31.3	1753
GEMS_N4636_14	1806	1.95	NGC 4536	...	12:34:27.13	02:11:16.4	1808
GEMS_N4636_15	1733	0.42	NGC 4496A	...	12:31:39.21	03:56:22.1	1730
GEMS_N4636_15	1733	0.50	SDSS J123139.98+035631.5	...	12:31:39.98	03:56:31.5	1747
GEMS_N4636_15	1733	0.86	NGC 4496	...	12:31:40.10	03:55:59.0	1738
GEMS_N4636_16	1731	2.40	IC 3474	...	12:32:36.51	02:39:41.5	1727
GEMS_N4636_17	2296	0.44	[IS196] 1228+0116	...	12:31:16.69	00:59:39.3	2289
GEMS_N4636_18	2472	2.75	SDSS J123402.06+014555.7	...	12:34:02.06	01:45:55.7	2502
GEMS_N4636_19	1632	1.17	VCC 1713	...	12:37:29.10	04:45:05.1	1655
GEMS_N4636_20	1070	4.23	NGC 4592	...	12:39:18.73	00:31:55.2	1069
GEMS_N4636_21	1518	3.69	2MASXi J1245041-002851	...	12:45:04.20	00:28:51.5	1679
GEMS_N4636_21	1518	3.22	[FNC2004] J124507.23-002740.3	...	12:45:07.23	00:27:40.3	1559
GEMS_N4636_21	1518	2.87	NGC 4666	...	12:45:08.68	00:27:42.9	1533
GEMS_N4636_21	1518	4.52	NGC 4668	...	12:45:31.99	00:32:08.6	1623
GEMS_N4636_21	1518	5.14	2QZ J124532.4-003253	...	12:45:32.46	00:32:52.9	1499
GEMS_N4636_21	1518	7.86	SDSS J124547.90-002556.1	...	12:45:47.90	00:25:56.1	1657
GEMS_N4636_22	1331	1.78	UGC 08041	...	12:55:12.65	00:07:00.0	1359

Table B5. Optical counterparts to the H I detections. The columns are the same as in Table B1.

(1)	(2)	(3)	(4)	(5)	(6)	(7)	(8)
GEMS_N5044_1 ⁴	3074	1.60	LEDA 083818	...	13:14:09.93	-16:41:41.6	...
GEMS_N5044_2	2928	4.12	NGC 5010	...	13:12:26.35	-15:47:52.3	2975
GEMS_N5044_3	2897	0.35	IC 4221	...	13:18:30.35	-14:36:32.0	2895
GEMS_N5044_4	2967	0.84	MCG -03-33-029	...	13:03:11.51	-17:22:33.4	2964
GEMS_N5044_5 ⁴	2912	2.10	[RC3] 1303.0-1530	...	13:05:37.27	-15:46:58.5	...
GEMS_N5044_6	2749	1.65	NGC 5073	...	13:19:20.65	-14:50:40.3	2744
GEMS_N5044_7	2828
GEMS_N5044_8	2753	0.73	MCG -03-34-014	...	13:12:35.43	-17:32:32.7	2760
GEMS_N5044_9	2773	1.49	ESO 576- G 017	J1315128-175800	13:15:12.80	-17:58:00.4	3006
GEMS_N5044_10 ^{1,4}	2748	1.87	[MMB2004] J1320-1427	...	13:20:13.00	-14:27:32.0	...
GEMS_N5044_11	2688	1.43	SGC 1317.2-1702	...	13:19:54.83	-17:18:55.8	2689
GEMS_N5044_12	2624	3.77	2MASX J13164875-1620397	J1316488-162040	13:16:48.75	-16:20:39.7	2619
GEMS_N5044_12	2624	3.16	MCG -03-34-041	...	13:17:06.13	-16:15:07.9	2628
GEMS_N5044_13	2694	3.12	MCG -03-34-020	...	13:13:12.48	-16:07:50.1	2663
GEMS_N5044_14 ⁴	2599	1.80	[RC3] 1305.5-1430	...	13:08:05.02	-14:44:53.3	...
GEMS_N5044_15	2572	1.9	PGC 045101	...	13:03:26.57	-14:46:08.0	2555
GEMS_N5044_16	2502	0.44	UGCA 338	...	13:13:34.34	-15:25:55.2	2503
GEMS_N5044_17	2494	0.98	SGC 1316.2-1722	...	13:18:56.50	-17:38:06.0	2495
GEMS_N5044_18 ⁴	2472
GEMS_N5044_19	2520	3.11	IC 0863	J1317124-171516	13:17:12.40	-17:15:16.1	2514
GEMS_N5044_20	1834	0.87	MCG -03-34-040	J1316562-163535	13:16:56.23	-16:35:34.7	2112
GEMS_N5044_20	1834	1.74	NGC 5054	...	13:16:58.49	-16:38:05.5	1741
GEMS_N5044_21	1924	2.4	UGCA 353	J1324418-194145	13:24:42.10	-19:41:49.8	1984
GEMS_N5044_22	2834	2.15	MCG -03-33-031	...	13:05:15.60	-16:53:19.0	2842
GEMS_N5044_23	2576	2.45	MCG -03-34-004	...	13:09:44.07	-16:36:07.6	2619
GEMS_N5044_23	2576	6.94	NGC 4997	...	13:09:51.70	-16:30:55.7	2376
GEMS_N5044_23	2576	7.13	6dF J1309535-163102	J1309535-163102	13:09:53.47	-16:31:01.6	2376

Table B6. Optical counterparts to the H I detections. The columns are the same as in Table B1.

(1)	(2)	(3)	(4)	(5)	(6)	(7)	(8)
GEMS_N7144_1 ⁴	1598	1.0	ESO 236- G 039	...	21:45:14.50	-49:00:32.0	...
GEMS_N7144_1 ⁴	1598	1.2	KTS 65	...	21:45:01.10	-49:00:36.0	...
GEMS_N7144_2	1722	1.52	NGC 7213	...	22:09:16.25	-47:10:00.0	1784
GEMS_N7144_2	1722	5.15	2MASX J22092496-4706129	J2209250-470613	22:09:24.98	-47:06:12.8	1787
GEMS_N7144_3	1617	0.00	ESO 236- G 041	...	21:45:49.10	-48:49:13.5	...
GEMS_N7144_4	1871	0.89	NGC 7151	...	21:55:03.72	-50:39:22.5	1859
GEMS_N7144_5 ⁴	1860	3.10	APMUKS(BJ) B215242.56-492853.8	...	21:55:56.92	-49:14:38.3	...
GEMS_N7144_6 ⁴	1956	3.97	ESO 236- G 035	...	21:42:43.71	-47:59:22.3	2086
GEMS_N7144_6 ⁴	1956	4.30	ESO 236- G 036	...	21:42:53.10	-47:51:28.0	...
GEMS_N7144_7 ⁴	1958	0.00	APMUKS(BJ) B213754.44-465227.8	...	21:41:09.10	-46:38:48.0	...
GEMS_N7144_8	2075	1.81	ESO 236- G 034	...	21:42:46.36	-51:17:12.4	2257
GEMS_N7714_1	2891	1.38	NGC 7731	...	23:41:29.07	03:44:24.1	2886
GEMS_N7714_1	2891	1.43	KPG 590	...	23:41:31.50	03:43:56.5	2801
GEMS_N7714_1	2891	1.81	NGC 7732	...	23:41:33.87	03:43:29.8	2907
GEMS_N7714_2	2721	2.95	NGC 7714	...	23:36:14.10	02:09:18.6	2798
GEMS_N7714_2	2721	1.99	ARP 284	...	23:36:18.11	02:09:21.3	2795
GEMS_N7714_2	2721	1.12	NGC 7715	...	23:36:22.08	02:09:24.1	2770
GEMS_N7714_3	2674	2.00	UGC 12709	...	23:37:24.02	00:23:30.1	2682
GEMS_N7714_4	2901	6.14	NGC 7750	...	23:46:37.84	03:47:59.3	2938
GEMS_N7714_5	2588	2.89	NGC 7716	...	23:36:31.46	00:17:50.3	2571
GEMS_N7714_6	2599	7.55	APMUKS(BJ) B233219.69+005549.2	...	23:34:53.31	01:12:24.8	2602
GEMS_N7714_7	2755
GEMS_HCG90_1	2271	2.49	ESO 404- G 018	...	22:01:10.16	-32:34:43.7	2268
GEMS_HCG90_2	2353	2.15	ESO 466- G 036	...	22:01:20.46	-31:31:46.9	2559
GEMS_HCG90_2	2353	1.92	2dFGRS S408Z202	...	22:01:21.44	-31:31:52.9	2457
GEMS_HCG90_3	2550	1.91	ESO 404- G 027	J2203478-321706	22:03:47.84	-32:17:06.0	2611
GEMS_HCG90_4	2583	1.76	NGC 7204	...	22:06:54.20	-31:03:05.0	2590
GEMS_HCG90_4	2583	1.54	NGC 7204B	...	22:06:55.26	-31:03:11.1	2590
GEMS_HCG90_5	2614	5.57	NGC 7154	...	21:55:21.04	-34:48:50.9	2616
GEMS_HCG90_6	2656	3.89	ESO 404- G 012	J2157072-343456	21:57:07.20	-34:34:55.7	2646
GEMS_HCG90_7	2515	7.00	ESO 404- G 017	J2200559-351713	22:00:55.87	-35:17:13.2	2478
GEMS_HCG90_8	2670	1.64	ESO 404- G?033	...	22:08:31.00	-34:17:04.2	2596
GEMS_HCG90_8	2670	1.50	2MASX J22083186-3417070	J2208317-341706	22:08:31.74	-34:17:05.9	2709
GEMS_HCG90_9	2720	3.05	IC 5156	J2203149-335018	22:03:14.87	-33:50:18.4	2709
GEMS_HCG90_10	2560	3.53	DUKST 467-039	...	22:08:38.24	-30:53:08.3	2613
GEMS_HCG90_11 ⁴	2596	2.17	ESO 467- G 002	J2206096-310518	22:06:09.60	-31:05:17.7	2521
GEMS_HCG90_11 ⁴	2596	7.64	NGC 7204	...	22:06:54.20	-31:03:05.0	2590
GEMS_HCG90_12	2316	3.74	NGC 7172	J2202019-315211	22:02:01.87	-31:52:11.1	2557
GEMS_HCG90_12	2316	4.78	NGC 7173	...	22:02:03.19	-31:58:25.3	2497
GEMS_HCG90_12	2316	4.20	2dFGRS S407Z097	...	22:02:04.81	-31:52:13.5	2384
GEMS_HCG90_12	2316	6.24	NGC 7176	J2202085-315923	22:02:08.45	-31:59:23.3	2503
GEMS_HCG90_12	2316	6.27	2dFGRS S407Z090	...	22:02:16.07	-31:57:11.8	2541

Table B7. Optical counterparts to the H I detections. The columns are the same as in Table B1.

(1)	(2)	(3)	(4)	(5)	(6)	(7)	(8)
GEMS_IC1459_1	1198	0.38	NGC 7456	J2302104-393410	23:02:10.37	-39:34:09.8	1187
GEMS_IC1459_2	1299	1.01	IC 5273	J2259267-374210	22:59:26.70	-37:42:10.4	1286
GEMS_IC1459_3	1239	1.01	ESO 406- G 040	...	23:00:22.18	-37:12:04.8	1248
GEMS_IC1459_4	1282	2.19	ESO 406- G 022	J2255526-343318	22:55:52.59	-34:33:17.8	1285
GEMS_IC1459_5	1372	0.26	ESO 406- G 042	...	23:02:14.21	-37:05:01.4	1375
GEMS_IC1459_6	1446	1.59	NGC 7418	J2256361-370148	22:56:36.13	-37:01:47.8	1417
GEMS_IC1459_7	1667	1.39	IC 5269B	J2256367-361459	22:56:36.72	-36:14:59.1	1638
GEMS_IC1459_8	1789	1.79	NGC 7421	J2256543-372050	22:56:54.33	-37:20:50.7	1801
GEMS_IC1459_9	1790	5.98	IC 5264	...	22:56:53.04	-36:33:15.0	1940
GEMS_IC1459_9	1790	7.73	IC 1459	J2257106-362744	22:57:10.61	-36:27:44.2	1713
GEMS_IC1459_9	1790	5.43	2MASX J22571092-3640103	...	22:57:10.92	-36:40:10.4	1945
GEMS_IC1459_10	1773	0.12	IC 5269C	...	23:00:48.55	-35:22:10.5	1796
GEMS_IC1459_11	1950	3.52	IC 5270	J2257549-355129	22:57:54.86	-35:51:28.5	1929
GEMS_IC1459_12	2101	2.11	NGC 7418A	...	22:56:41.15	-36:46:21.2	2102
GEMS_IC1459_12	2101	7.17	2MASX J22571092-3640103	...	22:57:10.92	-36:40:10.4	1945
GEMS_IC1459_13	2279	2.14	NGC 7368	J2245317-392031	22:45:31.68	-39:20:30.7	2355
GEMS_IC1459_14	2147	4.65	ESO 345- G 046	...	22:43:16.09	-39:51:58.9	2149
GEMS_IC1459_15	1718	1.42	IC 5271	...	22:58:01.82	-33:44:32.0	1738
GEMS_IC1459_16	1787	3.04	ESO 346- G 033	...	23:08:46.60	-39:48:42.7	1759
GEMS_IC1459_17	879	0.93	ESO 346- G 007	...	22:53:23.90	-38:47:58.4	928
GEMS_IC1459_18	1668	4.69	DUKST 406-083	...	23:02:00.49	-36:29:01.9	1624

¹⁻⁴ Sources have ATCA observations, and thus a confirmed optical counterpart (except in the case of GEMS_N3783.2 where no optical counterpart is seen). The references are:

¹ McKay et al. (2004)

² Kilborn et al. (2005)

³ Kilborn et al. (2006)

⁴ Kern et al. (2008)

* Velocity is a previous H I measurement associated with this galaxy.

** Previously catalogued optical counterpart is further than 8 arcminutes from the central H I position. Confirmation of optical counterpart is required.